Mechanism and Machine Theory 153 (2020) 103957

Contents lists available at ScienceDirect

Mechanism and Machine Theory

journal homepage: www.elsevier.com/locate/mechmachtheory

An approach for jerk-continuous trajectory generation of robotic manipulators with kinematical constraints

Yi Fang, Jin Qi, Jie Hu*, Weiming Wang, Yinghong Peng

School of Mechanical Engineering, Shanghai Jiao Tong University, Shanghai 200240, China

ARTICLE INFO

Article history:
Received 9 January 2020
Revised 12 April 2020
Accepted 17 May 2020
Available online 15 June 2020

Keywords:
Trajectory planning
Robot manipulator
Sine jerk
Kinematical constraint
Smooth motion

ABSTRACT

This paper proposes a methodology to generate online smooth joint trajectories of robots based on an improved sinusoidal jerk model. The multi-segment trajectory model is designed to allow a more sufficient exploitation of the actuation capability, thereby shortening the execution time while ensuring continuity up to the jerk level. Afterwards, the general mathematical expressions of the motion profiles are derived from integration of the jerk function. By analyzing the critical constraint conditions corresponding to each possible profile type, a complete closed-form solution to the minimum time planning problem with consideration of kinematic constraints has then been worked out, where a parameter named the ramp coefficient that manages the ratio of the sine jerk period is introduced to simplify the determination of the motion formulas. Thus the method results in a computationally light optimization procedure for facile implementation and enables a higher level of regularity for achieving desirable motion behaviours in light of the operation requirements and joint characteristics. Experimental results conducted on a robot manipulator reveal that the proposed approach is capable of yielding better performance than existing techniques in terms of efficiency and jerk suppression.

1. Introduction

In the modern manufacturing industry, due to their outstanding agility and adaptability, industrial robots have been increasingly implemented to substitute for human power to satisfy growing demands in terms of cost reduction, throughput increase and personal safety. As an essential research topic in the robotics field, trajectory planning has received intensive attention over the last few decades since it plays an important role in controlling a robot to accomplish a desired task. Generally, most current applications, such as automated assembly, spot welding, palletizing, drilling and material handling [1], require high-speed and precise operations for greater productivity and product quality, which are linked to economic implications. Moreover, manipulator systems present a tendency to develop from traditional heavy and rigid mechanical structures towards lightweight and flexible structures to promote energy savings [2]. In such cases, the robots are expected to perform not only swift but also smooth movements with low residual vibration and position overshoot [3]. However, shortening the execution time and maintaining motion smoothness usually represent a contradictory relation in trajectory design. Faster motions characterized by dramatic changes in velocity and acceleration would lead to stronger impact loads. Therefore, addressing the trade-off between the two aspects remains a challenging problem that needs further investigation.

* Corresponding author.
E-mail address: hujie@sjtu.edu.cn (J. Hu).

https://doi.org/10.1016/j.mechmachtheory.2020.103957
0094-114X/

The traditional time optimal motion laws with jumpwise acceleration, which focus mainly on maximizing efficiency from the temporal perspective, can excite structural resonance related to the chatter phenomenon, which is likely to damage the actuators and transmission components and consequently incur a large tracking error, making these laws physically difficult to implement on a machine in reality [4,5]. From the viewpoint of practical implementation, non-smooth trajectories should be avoided whenever possible because they necessitate abrupt joint torque variations that cannot be provided by the actuators. Improved motion control can be achieved by accurate dynamic modeling of the robot [6,7] or alternatively by forcing the planning module to generate trajectories featuring a sufficiently high level of continuity, preferably, at least up to the acceleration level such that the jerk (time derivative of the acceleration) is limited [8,9]. Additionally, the planned trajectories should meet specific constraints on position, velocity, acceleration and jerk values according to the mechanical characteristics of the driving apparatus to guarantee the dynamic performance of the system [13]. In fact, according to the types of constraints considered in trajectory planning, the methods can be categorized into kinematic and dynamic trajectory planning [10]. Dynamic approaches consider the full dynamic model of the manipulator and formulate an optimization problem with dynamic constraints, such as the limits of the actuator torques and torque variation rates (actuator jerks) [11]. Kinematic approaches express actuator constraints in terms of bounds related to torque, such as velocity, acceleration and jerk limits, rather than torque itself [12]. Each category of method has its own benefits and weaknesses. Considering dynamic constraints allows a better capacity utilization of the manipulator at the cost of a complex computational model due to the inherent nonlinearity. Applying only kinematic constraints leads to a simpler computational model with an underutilization of the full dynamic capabilities since the constant bounds must be chosen as the effective lower bounds for the worst case (maximum inertia) in the entire workspace, but this strategy still produces reasonably good solutions. Therefore, dynamic approaches are generally performed offline, while kinematic approaches are more suitable for online implementation. Regardless of the approach, the system is unlikely to accurately track the trajectory if the jerk limit is not considered. It has been widely accepted that jerk-bounded profiles have particular relevance to suppressing vibration and increasing tracking accuracy during movement, thus alleviating wear and prolonging the service life of the manipulator [14,15].

To date, aiming to achieve a smooth trajectory with limited jerk, polynomial functions satisfying some optimality criteria have been broadly applied as trajectory primitives in the vast scientific literature on this topic [16–20]. Most of the objective functions are related to the execution time, jerk or energy. Gallant and Gosselin [21] investigated the issue of enhancing the payload capacity of manipulators through optimization of cubic spline and Bernstein polynomial trajectories using a sequence quadratic program. In [22], a "3–4–5″ polynomial model was employed in conjunction with minimum jerk theory to create smooth human-like movements for assistive robots. However, the motion constraints were not considered. Ref. [23] suggested a time-optimal trajectory planning methodology based upon Pythagorean-hodograph curves for the pick-and-place operation of delta robots. Representing a motion equation by a quintic polynomial function, Bureerat et al. [24] obtained a minimum time-jerk trajectory subject to kinematic constraints. An approach to compute multi-objective optimal motions of an industrial manipulator was proposed in [25], where the joint temporal evolutions were parameterized via a cubic B-spline curve. In ref. [26], a genetic algorithm (GA)-based technique was developed to optimize the travelling time and space for point-to-point joint space trajectory planning of a 3-link redundant robot arm. However, these methods do not ensure the continuity of the jerk profile along the whole trajectory. As pointed out by [27], the undesirable jerk impulse appearing at the starting and ending points has a detrimental effect on the positioning accuracy.

To eliminate the disadvantageous jerk effect and attain a higher level of continuity and regularity, some works have attempted to build a trajectory by increasing the polynomial degree [28]. Seventh-order polynomial interpolation is commonly employed in pick-and-place operations of robots [29,30] and in high-precision positioning systems [31] to satisfy the jerk boundary conditions. On the basis of previous research on maximal dexterous trajectories for fully planar parallel manipulators [32], Kucuk [33] combined cubic splines and 7th-order polynomials to ensure zero jerk at the start and end points of joint movements. A particle swarm optimization algorithm was used to produce time optimal smooth motion trajectories. A methodology for smooth fifth-order B-spline trajectory planning with an objective function defined in terms of the travelling time and the integrated squared jerk was described in [34]. Sencer and Ishizaki [35] presented a frequency optimal motion profile generation technique to minimize the vibrations excited by the reference acceleration profile for high-speed motion systems, while ref. [36] focused on constructing a smooth and minimum time joint trajectory of robot manipulators under kinematic constraints. A point-to-point trajectory of an LCD glass-handing robot was designed in [37] through a polynomial of up to degree twelve using a real-coded GA with an energy fitness function. Despite an improved smoothness degree provided by high-order polynomial trajectories, they may suffer from a heavy computation load with degraded numerical accuracy. Solving a significant amount of polynomial coefficients is often an arduous procedure [38]. As a matter of fact, a generic polynomial of degree n has $n+1$ coefficients to be solved for characterizing the trajectory [39] and requires $n(n+1)/2$ multiplications and n additions to evaluate for a specific time value. Since polynomials higher than fourth order have no formula solution, the optimization of polynomial coefficients may entail an iterative routine such as the Newton-Raphson method or GA [40]. On the other hand, the higher-order terms involving multiple multiplication operations necessitate a large number of decimal digits of accuracy for the storing of data to guarantee the desired precision due to the truncation errors associated with floating-point operations [41]. For this purpose, the property of root multiplicity has been exploited by researchers to simplify the polynomial form. For instance, Wang et al. [42] planned the joint acceleration in the accelerated and decelerated parts with quartic polynomials, for which only one coefficient needs to be determined.

Another category of widespread approaches in the numerical control system consists of incorporating the trigonometric functions into the motion laws to enhance the ease of their implementation [43,44]. For a flexible dual manipulator, Abe and Hashimoto [45] put forward a feedforward control technique that adopts a cycloidal function taking a polynomial function as input to generate trajectories with suppressed residual vibrations in point-to-point motion. An approach ensuring continuity of the first three derivatives is described in [46], where a robot joint trajectory is interpolated by minimum jerk trigonometric splines. This study considers an execution time set a priori and does not accept any kinematic constraint as input. Lee et al. [47] developed an offline feedrate scheduling algorithm taking into account the chord tolerance, acceleration and jerk limits for parametric interpolators in machine tools with the use of a sine-curve velocity profile, where the jerk has a jump at the start and end of the acceleration and deceleration phases. A conceptually different technique is presented in [48], where the trigonometric trajectories compliant with several kinematic constraints are generated online by means of a cascade of rectangular and harmonic filters for vibration suppression. However, this method considers only single-axis motion under the condition that the trajectory reaches all the kinematic bounds for time optimality. In [49], trigonometric velocity scheduling was presented to realize continuous velocity, acceleration, and jerk control in high-accuracy machining. Similarly, the generation of a smooth and time-optimal trajectory in joint space for a 6-DOF robot was studied in [50] utilizing a continuous jerk profile with a sine wave template. Although the numerical examples showed the superiority of this method in execution time and jerk values over spline-based methods, the method presents some deficiencies. The feasibility of the motion profiles developed cannot be guaranteed with certainty because the bounds on velocity are ignored. Additionally, the synchronization strategy for the joint movements not only limits the capability in leveraging the characteristics of joint motors, resulting in unnecessary prolongation of the execution time, but also invalidates the algorithm in the presence of a constant velocity phase. Subsequently, Valente et al. [51] applied a multi-variable time optimization approach to achieve the best admissible performance for trajectory planning based on the same kind of jerk profile in [50] while overcoming the abovementioned shortcomings. However, the single sine function employed for this profile during the acceleration/deceleration phases actually leads to conservative velocity control in a sense and consequently to a loss of efficiency. Furthermore, a numerical technique, such as an active-set algorithm, is needed to solve the optimization problem, which can be a time-consuming process. Since industrial robots and numerical control devices usually require real-time implementation of motion profiles on inexpensive processors, simple planning algorithms with low computational complexity are favored for practical use.

Motivated by the above work, the principal purpose of this study is to suggest a novel motion profile generation method by using a trigonometric jerk model for applications of industrial robotic manipulators with the requirements of rapidity and high accuracy. Compared to current sine jerk-based schemes, the present method introduces several distinctive features: First, the developed model subdivides the entire trajectory into more delicate segments to speed up the acceleration/deceleration process, thereby possibly contributing to more efficient movements. Second, to avoid numerical complexity that may not be preferred in the actual engineering field, the time optimization of the overall motion under kinematical constraints is achieved analytically through the establishment of constraint criteria without relying on any iterative procedure, while the solution is always reliable to provide feasible trajectories. Moreover, the trade-off between rapidity and motion smoothness is adjustable via a designed parameter, making the approach more adaptable for the needs of different task demands.

The rest of this paper is organized as follows: Section II first briefly discusses the advantages and shortcomings of the sine jerk model previously presented in the literature. After that, the proposed smooth jerk motion profile and its mathematical formulations are detailed. This is followed in Section III by the introduction of an algorithm for obtaining optimal motion parameters with specified constraints. Then, the experimental results and analysis are described in Section IV, and finally, Section V gives conclusions and describes potential future work.

2. General formulation for the sine-jerk motion profile

The method described in this study mainly aims at planning trajectories in joint space for agile and smooth point-to-point movements requiring precise positioning with a free path. The execution time of the motion profiles between desired joint configurations is optimized taking into account kinematic constraints on the velocity, acceleration and jerk of the robot joints. As the joint angular rates and the Cartesian velocities of the end-effector are associated straightforwardly through the Jacobian matrix $\mathbf{J}_a$, the generalized velocity, acceleration and jerk of the end-effector can be derived based on the this matrix and its time derivatives:

$$\begin{aligned}\hat{\mathbf{v}}_e &= \mathbf{J}_a(\mathbf{q})\dot{\mathbf{q}}\\ \hat{\mathbf{a}}_e &= \dot{\mathbf{J}}_a(\mathbf{q})\dot{\mathbf{q}} + \mathbf{J}_a(\mathbf{q})\ddot{\mathbf{q}}\\ \hat{\mathbf{j}}_e &= \ddot{\mathbf{J}}_a(\mathbf{q})\dot{\mathbf{q}} + 2\dot{\mathbf{J}}_a(\mathbf{q})\ddot{\mathbf{q}} + \mathbf{J}_a(\mathbf{q})\dddot{\mathbf{q}}\end{aligned} \tag{1}$$

where $\mathbf{q}$ is the joint input variable vector of the robot. By inspection of the above formulas, it is recognized that the smoothness of the joint trajectories inherently implies continuous tip trajectories in the operational space, and vice versa in the absence of singularities [9].

Since this method is essentially a control strategy for the motion law acting at the joint level, which is independent of the number of joints and link geometries, it can theoretically be adapted to different industrial manipulators provided that the desired points and the corresponding kinematic limits are given in joint space. In the case of a flexible structure,

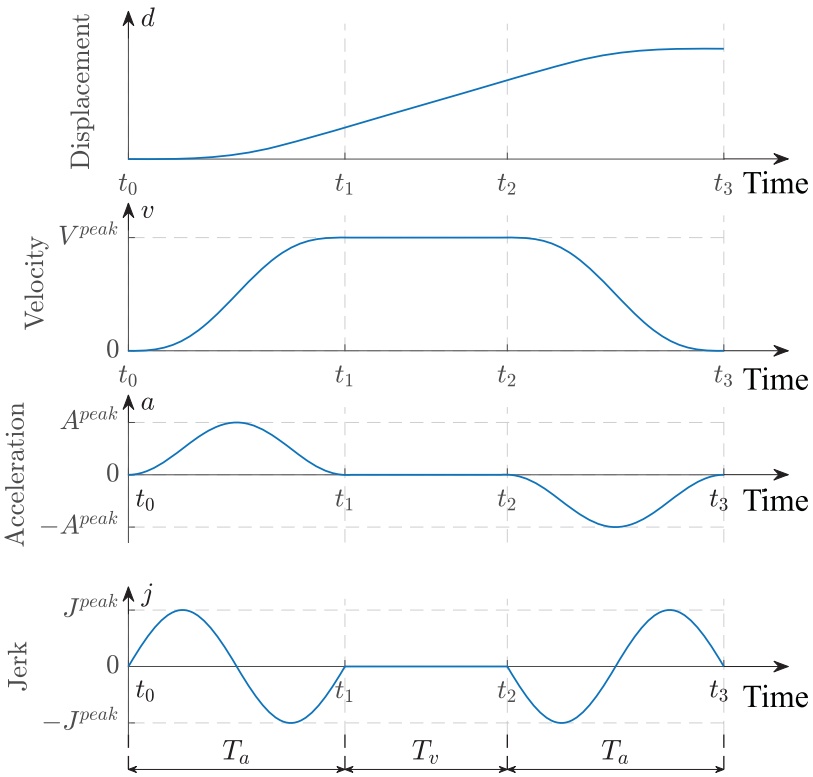

Fig. 1. Motion profiles of the canonical 3-phase sinusoidal jerk model.

a smooth trajectory with higher order continuity may not excite high-frequency modes of the system, thus resulting in motion with less vibration. Here, it is assumed that no obstacle collision occurs during the movement in the workspace, and an additional path planning process may be performed beforehand to set collision-free waypoints or configurations according to environmental knowledge. This section will be devoted to first outlining the sine jerk trajectory model found in relevant previous literature with a discussion of its advantages and limitations, and then presenting the proposed motion profile and its formulations.

2.1. Three-phase sine jerk motion profile

The three-phase sine jerk profile was initially suggested in [52] for linear motion stages and has since been adopted for trajectory generation of industrial articulated robots [50,51] as well as of machine tools [53]. The profile is comprised of symmetrical accelerating and decelerating phases connected by a constant velocity phase. As illustrated in Fig. 1, the jerk curves during the accelerating and decelerating phases are derived from a single sinusoidal function expressed as follows:

$$j(t) = \begin{cases} J^{peak} \sin\left[\frac{2\pi}{T_a}(t - t_0)\right] & t_0 \le t \le t_1 \\ 0 & t_1 \le t \le t_2 \\ -J^{peak} \sin\left[\frac{2\pi}{T_a}(t - t_2)\right] & t_2 \le t \le t_3 \end{cases} \tag{2}$$

where J^{peak} denotes the peak jerk value and $T_a = t_1 - t_0 = t_3 - t_2$ is the acceleration/deceleration time. Correspondingly, the acceleration curve varies in a level-shifted cosinusoidal waveform.

One benefit of this profile is its succinct formulation, which enables a simple algorithmic implementation. All kinematic trajectories are defined by only a few parameters, whose values are optimized based on the bounds imposed on velocity, acceleration and jerk. In addition, this trajectory model exhibits a continuous jerk curve without any sudden change such that transient vibration can be further mitigated compared to the profile with piecewise constant jerks [52].

However, the main weakness of this profile lies in that the jerk and acceleration cannot remain at their maximum values due to the single sine wave variation in the jerk profile. Indeed, since the key quantities (peak jerk, acceleration, velocity) are parametrized as functions of two variables to be optimized, i.e., the total motion time and the acceleration time, even though the upper bounds for the three quantities are specified, only part of them are active; in other words, it is ordinarily impossible to reach all the kinematic limits during movement. As a result, the physical capabilities of the machine are not exploited in a truly effective manner, corresponding to degradation in the operating efficiency.

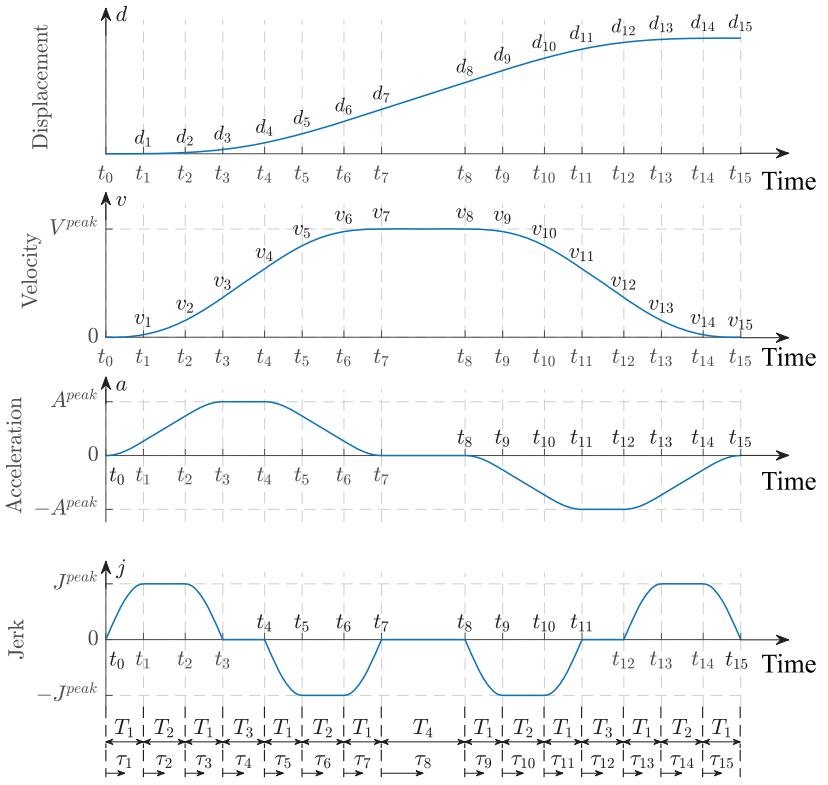

Fig. 2. Motion profiles of the proposed 15-phase sinusoidal jerk model.

2.2. Proposed modified sine jerk motion profile

With the above factors in mind, a modified sine jerk model is designed to enable a fuller utilization of physical limits of the drives, with consequent shortening of the execution time. The basic idea consists of keeping the kinematic quantities in the saturation state for the longest possible time to maximize the constant velocity phase. With respect to the canonical sine jerk model, this model extends to fifteen trajectory segments as the phases of constant peak jerk and acceleration have been included in the accelerating/decelerating sections while the jerk continuity is still preserved. Fig. 2 depicts the graphical representation of its displacement, velocity, acceleration and jerk profiles. Here, t_i $(i = 0,\ 1,\ \cdots,\ 15)$ is the time boundary of each segment; d_i and v_i $(i = 0,\ 1,\ \cdots,\ 15)$ respectively represent the displacement and velocity reached at the end of the ith segment; and J^{peak}, A^{peak} and V^{peak} respectively denote the peak values of jerk, acceleration and velocity during the motion.

The complete model now consists of eight sine jerk phases, four constant jerk phases, two constant acceleration phases and one constant velocity phase. Accordingly, a trajectory can be fully described with four time parameters T_1, T_2, T_3 and T_4, which represent the corresponding durations for the four types of phases. By regulation of these time parameters, it is easy to control the maximum kinematic values. The jerk profile displayed in Fig. 2 is expressed as the following piecewise trigonometric function:

$$j(t) = \begin{cases} J^{peak}\sin\left(\frac{\pi}{2T_1}\tau_i\right), & t_0 \le t < t_1,\ t_{12} \le t < t_{13} \\ J^{peak}, & t_1 \le t < t_2,\ t_{13} \le t < t_{14} \\ J^{peak}\sin\left[\frac{\pi}{2}\left(1+\frac{\tau_i}{T_1}\right)\right], & t_2 \le t < t_3,\ t_{14} \le t \le t_{15} \\ 0, & t_3 \le t < t_4,\ t_7 \le t < t_8,\ t_{11} \le t < t_{12} \\ -J^{peak}\sin\left(\frac{\pi}{2T_1}\tau_i\right), & t_4 \le t < t_5,\ t_8 \le t < t_9 \\ -J^{peak}, & t_5 \le t < t_6,\ t_9 \le t < t_{10} \\ -J^{peak}\sin\left[\frac{\pi}{2}\left(1+\frac{\tau_i}{T_1}\right)\right], & t_6 \le t < t_7,\ t_{10} \le t < t_{11} \end{cases} \tag{3}$$

where $\tau_i = t - t_i$ represents the relative time that starts from the beginning of the ith interval $[t_i,\ t_{i+1}]$ $(i = 1,\ 2,\ \ldots,\ 15)$. The corresponding acceleration, velocity and displacement profiles can be readily derived by sequentially integrating the

jerk function based on the initial conditions of each segment:

$$\begin{cases} a(t) = a(t_i) + \int_{t_i}^{t} j(t)dt \\ v(t) = v(t_i) + \int_{t_i}^{t} a(t)dt \\ d(t) = d(t_i) + \int_{t_i}^{t} v(t)dt \end{cases} \tag{4}$$

During the acceleration stage, for $t \in [t_0, t_1]$,

$$\begin{cases} a(t) = \frac{2J^{peak}T_1}{\pi}\left[1 - \cos\left(\frac{\pi}{2T_1}\tau_1\right)\right] \\ v(t) = \frac{2J^{peak}T_1}{\pi}\tau_1 - J^{peak}\left(\frac{2T_1}{\pi}\right)^2 \sin\left(\frac{\pi}{2T_1}\tau_1\right) \\ d(t) = \frac{J^{peak}T_1}{\pi}{\tau_1}^2 - J^{peak}\left(\frac{2T_1}{\pi}\right)^3\left[1 - \cos\left(\frac{\pi}{2T_1}\tau_1\right)\right] \end{cases} \tag{5}$$

For $t \in [t_1, t_2]$,

$$\begin{cases} a(t) = \frac{2J^{peak}T_1}{\pi} + J^{peak}\tau_2 \\ v(t) = v_1 + \frac{2J^{peak}T_1}{\pi}\tau_2 + \frac{1}{2}J^{peak}{\tau_2}^2, \text{ where } v_1 = J^{peak}\left[\frac{{2T_1}^2}{\pi} - \left(\frac{2T_1}{\pi}\right)^2\right] \\ d(t) = d_1 + J^{peak}\left[\frac{{2T_1}^2}{\pi} - \left(\frac{2T_1}{\pi}\right)^2\right]\tau_2 + \frac{J^{peak}T_1}{\pi}{\tau_2}^2 + \frac{1}{6}J^{peak}{\tau_2}^3, \text{ where } d_1 = J^{peak}\left[\frac{{T_1}^3}{\pi} - \left(\frac{2T_1}{\pi}\right)^3\right] \end{cases} \tag{6}$$

For $t \in [t_2, t_3]$,

$$\begin{cases} a(t) = \frac{2J^{peak}T_1}{\pi} + J^{peak}T_2 + \frac{2J^{peak}T_1}{\pi}\sin\left(\frac{\pi}{2T_1}\tau_3\right) \\ v(t) = v_2 + J^{peak}\left(\frac{2T_1}{\pi} + T_2\right)\tau_3 - J^{peak}\left(\frac{2T_1}{\pi}\right)^2\cos\left(\frac{\pi}{2T_1}\tau_3\right), \text{ where } v_2 = J^{peak}\left(\frac{{2T_1}^2}{\pi} + \frac{2T_1T_2}{\pi} + \frac{{T_2}^2}{2}\right) \\ d(t) = d_2 + J^{peak}\left(\frac{{2T_1}^2}{\pi} + \frac{2T_1T_2}{\pi} + \frac{{T_2}^2}{2}\right)\tau_3 + \frac{1}{2}J^{peak}\left(\frac{2T_1}{\pi} + T_2\right){\tau_3}^2 - J^{peak}\left(\frac{2T_1}{\pi}\right)^3\sin\left(\frac{\pi}{2T_1}\tau_3\right), \\ \text{where } d_2 = J^{peak}\left[\frac{{T_1}^3}{\pi} - \left(\frac{2T_1}{\pi}\right)^3 + \frac{2{T_1}^2T_2}{\pi} - \left(\frac{2T_1}{\pi}\right)^2T_2 + \frac{T_1{T_2}^2}{\pi} + \frac{{T_2}^3}{6}\right] \end{cases} \tag{7}$$

Note that the peak value of acceleration occurs at $t = t_3$ and is represented by:

$$A^{peak} = a(t_3) = J^{peak}\left(\frac{4T_1}{\pi} + T_2\right) \tag{8}$$

For $t \in [t_3, t_4]$,

$$\begin{cases} a(t) = A^{peak} \\ v(t) = v_3 + A^{peak}\tau_4, \text{ where } v_3 = A^{peak}\left(T_1 + \frac{T_2}{2}\right) \\ d(t) = d_3 + \frac{A^{peak}}{2}(2T_1 + T_2)\tau_4 + \frac{1}{2}A^{peak}{\tau_4}^2, \text{ where } d_3 = J^{peak}\left(\frac{{4T_1}^3}{\pi} - \frac{16{T_1}^3}{\pi^3} + \frac{{T_1}^2T_2}{2} + \frac{4{T_1}^2T_2}{\pi} - \frac{4{T_1}^2T_2}{\pi^2} + \frac{T_1{T_2}^2}{2} + \frac{T_1{T_2}^2}{\pi} + \frac{{T_2}^3}{6}\right) \end{cases} \tag{9}$$

For $t \in [t_4, t_5]$,

$$\begin{cases} a(t) = A^{peak} - \frac{2J^{peak}T_1}{\pi}\left[1 - \cos\left(\frac{\pi}{2T_1}\tau_5\right)\right] \\ v(t) = v_4 + \left(A^{peak} - \frac{2J^{peak}T_1}{\pi}\right)\tau_5 + J^{peak}\left(\frac{2T_1}{\pi}\right)^2\sin\left(\frac{\pi}{2T_1}\tau_5\right), \text{where } v_4 = A^{peak}\left(T_1 + \frac{T_2}{2} + T_3\right) \\ d(t) = d_4 + A^{peak}\left(T_1 + \frac{T_2}{2} + T_3\right)\tau_5 + \frac{1}{2}\left(A^{peak} - \frac{2J^{peak}T_1}{\pi}\right){\tau_5}^2 + J^{peak}\left(\frac{2T_1}{\pi}\right)^3\left[1 - \cos\left(\frac{\pi}{2T_1}\tau_5\right)\right], \\ \text{where } d_4 = A^{peak}\left(T_1T_3 + \frac{T_2T_3}{2} + \frac{{T_2}^2}{2}\right) + J^{peak}\left(\frac{{4T_1}^3}{\pi} - \frac{16{T_1}^3}{\pi^3} + \frac{{T_1}^2T_2}{2} + \frac{4{T_1}^2T_2}{\pi} - \frac{4{T_1}^2T_2}{\pi^2} + \frac{T_1{T_2}^2}{2} + \frac{T_1{T_2}^2}{\pi} + \frac{{T_2}^3}{6}\right) \end{cases} \tag{10}$$

For $t \in [t_5, t_6]$,

$$\begin{cases} a(t) = A^{peak} - \frac{2J^{peak}T_1}{\pi} - J^{peak}\tau_6 \\ v(t) = v_5 + \left(A^{peak} - \frac{2T_1}{\pi}J^{peak}\right)\tau_6 - \frac{1}{2}J^{peak}{\tau_6}^2, \text{where } v_5 = A^{peak}\left(2T_1 + \frac{T_2}{2} + T_3\right) + J^{peak}\left[\left(\frac{2T_1}{\pi}\right)^2 - \frac{{2T_1}^2}{\pi}\right] \\ d(t) = d_5 + A^{peak}\left(2T_1 + \frac{T_2}{2} + T_3\right)\tau_6 + J^{peak}\left[\left(\frac{2T_1}{\pi}\right)^2 - \frac{{2T_1}^2}{\pi}\right]\tau_6 + \frac{1}{2}\left(A^{peak} - \frac{2J^{peak}T_1}{\pi}\right){\tau_6}^2 - \frac{1}{6}J^{peak}{\tau_6}^3, \\ \text{where } d_5 = A^{peak}\left(\frac{3}{2}{T_1}^2 + \frac{T_1T_2}{2} + 2T_1T_3 + \frac{T_2T_3}{2} + \frac{{T_3}^2}{2}\right) + J^{peak}\left(\frac{3{T_1}^3}{\pi} - \frac{8{T_1}^3}{\pi^3} + \frac{{T_1}^2T_2}{2} + \frac{4{T_1}^2T_2}{\pi} - \frac{4{T_1}^2T_2}{\pi^2} + \frac{T_1{T_2}^2}{2} + \frac{T_1{T_2}^2}{\pi} + \frac{{T_2}^3}{6}\right) \end{cases} \tag{11}$$

For $t \in [t_6, t_7]$,

$$\begin{cases} a(t) = A^{peak} - J^{peak}\left(\frac{2T_1}{\pi} + T_2\right) - \frac{2J^{peak}T_1}{\pi}\sin\left(\frac{\pi}{2T_1}\tau_7\right) \\ v(t) = v_6 + \frac{2J^{peak}T_1}{\pi}\tau_7 + J^{peak}\left(\frac{2T_1}{\pi}\right)^2\cos\left(\frac{\pi}{2T_1}\tau_7\right), \text{ where } v_6 = A^{peak}\left(2T_1 + \frac{3T_2}{2} + T_3\right) - J^{peak}\left(\frac{2{T_1}^2}{\pi} + \frac{2T_1T_2}{\pi} + \frac{{T_2}^2}{2}\right) \\ d(t) = d_6 + A^{peak}\left(2T_1 + \frac{3T_2}{2} + T_3\right)\tau_7 - J^{peak}\left(\frac{2{T_1}^2}{\pi} + \frac{2T_1T_2}{\pi} + \frac{{T_2}^2}{2}\right)\tau_7 + \frac{J^{peak}T_1}{\pi}{\tau_7}^2 + J^{peak}\left(\frac{2T_1}{\pi}\right)^3\sin\left(\frac{\pi}{2T_1}\tau_7\right), \\ \text{where } d_6 = A^{peak}\left(2T_1T_2 + {T_2}^2 + \frac{3}{2}{T_1}^2 + \frac{T_1T_2}{2} + 2T_1T_3 + \frac{3}{2}T_2T_3 + \frac{{T_3}^2}{2}\right) + J^{peak}\left(\frac{3{T_1}^3}{\pi} - \frac{8{T_1}^3}{\pi^3} + \frac{{T_1}^2T_2}{2} + \frac{2{T_1}^2T_2}{\pi} + \frac{T_1{T_2}^2}{2}\right) \end{cases} \tag{12}$$

The peak velocity is reached when the acceleration completes its positive phase, i.e., $t = t_7$, and can be identified as:

$$V^{peak} = v_7 = A^{peak}(2T_1 + T_2 + T_3) = J^{peak}\left(\frac{8{T_1}^2}{\pi} + \frac{4T_1T_2}{\pi} + \frac{4T_1T_3}{\pi} + 2T_1T_2 + {T_2}^2 + T_2T_3\right) \tag{13}$$

For the constant velocity phase $t \in [t_7, t_8]$,

$$\begin{cases} a(t) = 0 \\ v(t) = V^{peak} \\ d(t) = d_7 + V^{peak}\tau_8, \text{ where } d_7 = V^{peak}\left(2T_1 + T_2 + \frac{T_3}{2}\right) \end{cases} \tag{14}$$

The formulations for the deceleration stage can be similarly achieved without difficulty, and they are omitted here for space reasons. The terminal displacement at the end time of the movement is given by:

$$\begin{aligned} d_{15} &= V^{peak}(4T_1 + 2T_2 + T_3 + T_4) = A^{peak}\left(8{T_1}^2 + 8T_1T_2 + 6T_1T_3 + 2T_1T_4 + 2{T_2}^2 + 3T_2T_3 + T_2T_4 + {T_3}^2 + T_3T_4\right) \\ &= J^{peak}\left(\begin{array}{l} \frac{32{T_1}^3}{\pi} + 8{T_1}^2T_2 + \frac{32{T_1}^2T_2}{\pi} + 8T_1{T_2}^2 + \frac{8T_1{T_2}^2}{\pi} + 2{T_2}^3 + \frac{24{T_1}^2T_3}{\pi} + \frac{12T_1T_2T_3}{\pi} + 6T_1T_2T_3 \\ +3{T_2}^2T_3 + \frac{4T_1{T_3}^2}{\pi} + T_2{T_3}^2 + \frac{8{T_1}^2T_4}{\pi} + \frac{4T_1T_2T_4}{\pi} + \frac{4T_1T_3T_4}{\pi} + 2T_1T_2T_4 + {T_2}^2T_4 + T_2T_3T_4 \end{array}\right) \end{aligned} \tag{15}$$

A sufficient condition for a time optimal trajectory is that the magnitudes of peak values of each kinematic variable during the motion are equal to their maximum allowable values. However, as discussed later, the phases of constant derivatives except the sine jerk phase could disappear, and the corresponding limit values cannot be attained under certain system constraints, which indicates that special cases corresponding to diverse possible trajectory shapes will occur in actual applications.

3. Trajectory optimization

Given the start and end points $\mathbf{P}_s = [q_{s,1},\ q_{s,2},\ \dots,\ q_{s,n}]$ and $\mathbf{P}_e = [q_{e,1},\ q_{e,2},\ \dots,\ q_{e,n}]$of a movement, where n is the number of robot joints and q represents the joint input variables, the aim of trajectory optimization is to find a set of optimum values for the time parameters of each joint such that the execution time is minimized while satisfying actuation constraints (maximum allowable joint velocity, acceleration and jerk $V_j^{\max}$, $A_j^{\max}$ and $J_j^{\max}$, $j = 1, 2, \dots, n$). Specifically, n joints must be considered simultaneously, and each joint normally has different constraint ranges depending on the associated links in the chain. The total travelling time for joint j is the sum of trajectory segment durations: $T_{joint,j} = 8T_{1,j} + 4T_{2,j} + 2T_{3,j} + T_{4,j}$. To achieve a coordinated global robot motion, it is expected that all joints are synchronized to start and end their movements simultaneously, which also alleviates unnecessary stress to the actuators and is necessary for controlled path (e.g., straight-line) motion. In addition, the values of time periods should guarantee that the resulting peak values of kinematic quantities are no larger than their maximum permissible values. Let $D_j = |q_{e,j} - q_{s,j}|$ denote the target displacement for joint j, defined as the absolute value of the total distance to travel between the initial and the terminal positions, and let T_m denote the overall execution time. The problem is then formulated mathematically as follows:

Minimize the objective function:

$$F_{obj}(\mathbf{T}) = T_m \quad j = 1,\ 2,\ \cdots,\ n \tag{16}$$

subject to:

$$\begin{cases} T_{joint,j} = T_m \\ \left|V_j^{peak}\right| = \frac{D_j}{f_1\left(T_{1,j},\ T_{2,j},\ T_{3,j},\ T_{4,j}\right)} \le V_j^{\max} \\ \left|A_j^{peak}\right| = \frac{D_j}{f_2\left(T_{1,j},\ T_{2,j},\ T_{3,j},\ T_{4,j}\right)} \le A_j^{\max} \\ \left|J_j^{peak}\right| = \frac{D_j}{f_3\left(T_{1,j},\ T_{2,j},\ T_{3,j},\ T_{4,j}\right)} \le J_j^{\max} \end{cases} \quad \forall j = 1,\ 2,\ \cdots,\ n \tag{17}$$

where $\mathbf{T} = [T_{1,j},\ T_{2,j},\ T_{3,j},\ T_{4,j}] \in [0,\ +\infty)$ $(j = 1, 2, \cdots, n)$ is the vector of time variables to be designed; f_1, f_2 and f_3 are the corresponding coefficient functions of the time parameters that relate the peak kinematic values to the terminal displacement in Eq. (15).

This nonlinear constrained optimization problem may be solved numerically as in [51] by reparametrizing the key quantities as functions of the total motion time T_m and the $3n$ phase durations $T_{1,j}$, $T_{2,j}$ and $T_{3,j}$. Since the total move is composed of four types of phases, the constant velocity phase $T_{4,j}$ can be expressed as $T_{4,j} = T_m - 8T_{1,j} - 4T_{2,j} - 2T_{3,j}$. Substituting this relation into Eq. (17) allows us to take into account the motion profiles of all joints at once, and the optimization variables are actually converted into $[T_m,\ T_{2,j},\ T_{3,j},\ T_{4,j}] \in [0,\ +\infty)$ in that case. However, this numerical treatment involves an iterative process and has the potential to fail due to an unsuitable initial solution. To relieve the computation burden of the controller and ensure the reliability for online implementation, this paper addresses the problem from another perspective, in which the whole procedure is divided into two stages: In the first stage, each joint is separately evaluated to obtain its individual minimum time trajectory. Since the displacement requirements and motion constraints are different for the joints, these trajectories also have, in general, different durations $T^{\min}_{joint,j}$. Of those various values of $T^{\min}_{joint,j}$, the largest is the shortest possible time T_m required to complete the overall motion. Then, in the second stage, the joints that have shorter $T^{\min}_{joint,j}$ are properly coordinated to adapt to the common movement time T_m.

Note that for an individual joint, the minimization of its traversal time signifies that the bounds on all considered trajectory derivatives need to be attained in succession from higher to lower order with the greatest rapidity, which is realized by driving the motion to its saturated limit condition during each trajectory segment. Therefore, it is essential to implement the trajectory with the jerk bound $J^{\max}$ in any circumstance; i.e., $|J^{peak}| = J^{\max}$ (if $q_e \geq q_s$, $J^{peak} = J^{\max}$; otherwise, $J^{peak} = -J^{\max}$) since the jerk serves as the highest controlled derivative for the proposed model, while the reachability of the other kinematic bounds relies upon the relationship among the target displacement and the bounds themselves because lower-order constraints actually form the restriction to the periods of higher derivatives. In this work, by analyzing the critical conditions based on system constraints, the actual trajectory shape can be predicted according to the established constraint criteria. As a consequence, closed-form solutions for all potential instances are derived to provide a straightforward designation of motion parameters, thus allowing real-time planning of reference trajectories. Once the minimum execution times for all joints are obtained, the original calculated parameters of faster joint trajectories are readjusted for compatibility with the slowest one. The flowchart summarizing the procedure of trajectory optimization for multiple joints is shown in Fig. 3, and the details are illustrated in the following passages.

3.1. Ramp coefficient

As described before, four time periods are to be calculated when generating a motion profile, and three relevant equations are available on the basis of the given trajectory requirements. The three equations establish the relationships between the time parameters and the corresponding three motion conditions (acceleration bound, velocity bound and target displacement). Since the constant jerk phase is introduced into the proposed trajectory model and the jerk constraint is the highest-order derivative constraint, the execution time is minimized if the constant jerk phases completely replace the sine jerk phases. Thus, solving the optimization problem with the existing constraints always obtains a solution with T_1 being zero, which is unexpected, as it produces discontinuous jerk at the boundaries of each trajectory segment. This may be avoided by additionally setting the constraint for the derivative of the jerk. However, it is not intuitive to manage the jerk profile shape in this way. To this end, let us introduce another parameter α, which is represented by the ratio of the sine jerk time period to the sum of the sine and constant jerk time periods of the trajectory:

$$\alpha = \frac{T_1}{T_1 + T_2} \tag{18}$$

It is evident that the value of this parameter varies in the range of 0 to 1. When $\alpha = 0$, it has $T_1 = 0$, the sine jerk segments disappear, and the trajectory retrogrades to the bang-bang jerk trajectory whose jerk curve is of rectangular form. $\alpha = 1$ signifies that $T_2 = 0$, i.e., the constant jerk segments are non-existent. At this point, the trajectory evolves into a seven-phase type with half-sine jerk pulses (Fig. 4). Intuitively, increasing α enhances the smoothness degree of movement at the cost of a longer motion completion time, and a smaller α indicates that the minimization of execution time tends to be given a higher priority. One can obtain different trajectories with the desired smoothness via adjusting the value of α. This feature provides flexibility for robots to accommodate various types of production tasks with specific requirements. Besides, the introduction of α facilitates the determination of motion parameters to some extent because it in effect lessens the number of independent parameters. Since both the system structures and the controllers of machines, together with the nature of tasks and other factors can vary, there does not exist a fixed common rule to choose α. Generally, if the robots feature high stiffness and quick response with time rather than precision being a primary aspect, the value of α may be selected as zero, while for the contrary case, a value closer to 1 would be more appropriate. A more ideal value can be determined experimentally. Here, to ensure a continuous jerk profile, the value of α is chosen within (0, 1] and taken to be the same for all joints. In what follows, this parameter is referred to as the ramp coefficient.

3.2. Minimum time trajectory for one joint

In order to determine the synchronized motion time, it is needed first to calculate the time optimal trajectories for each joint. The joint index j is dropped in the formulas of this subsection for the sake of notational brevity, as all joints are

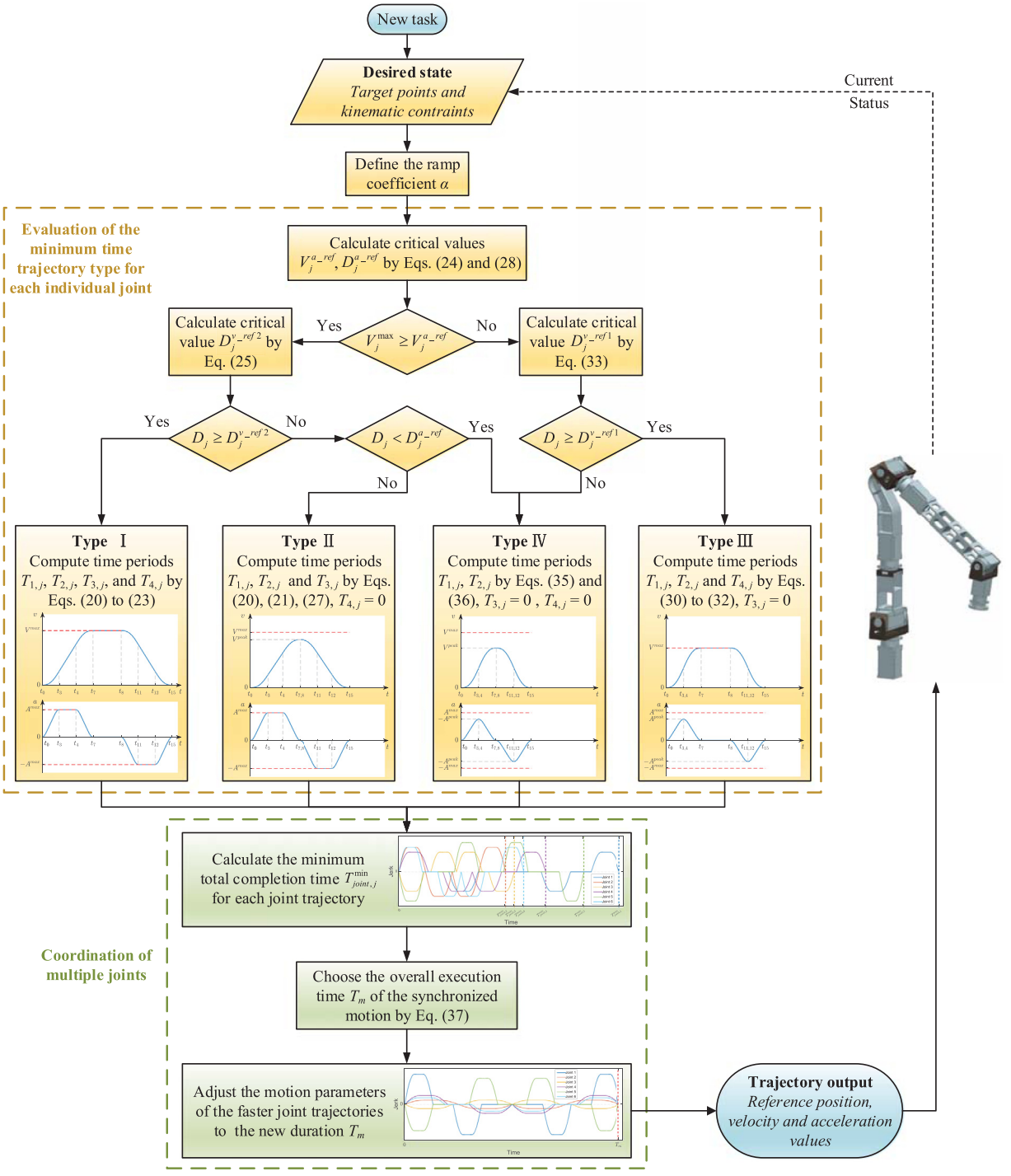

Fig. 3. Flowchart of the proposed trajectory planning methodology.

treated separately in the same way. From Eq. (18), T_2 may be written as a function of T_1:

$$T_2 = \frac{(1-\alpha)T_1}{\alpha}(\alpha \neq 0) \tag{19}$$

After specifying the ramp coefficient, only three time periods remain to be determined. The sine jerk time period T_1 must exist in the trajectory, as does T_2 if $\alpha \neq 1$. The constant acceleration time period T_3 may disappear because of the short

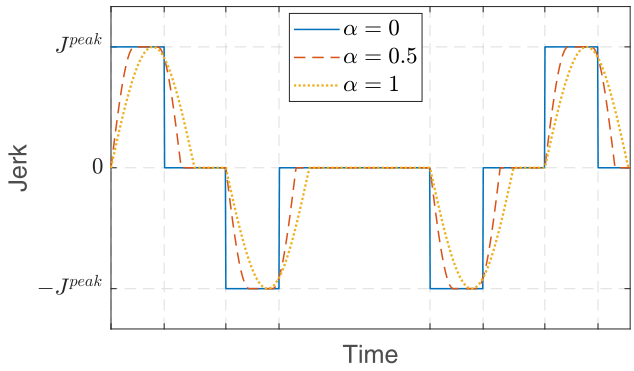

Fig. 4. Jerk shapes with different values of α.

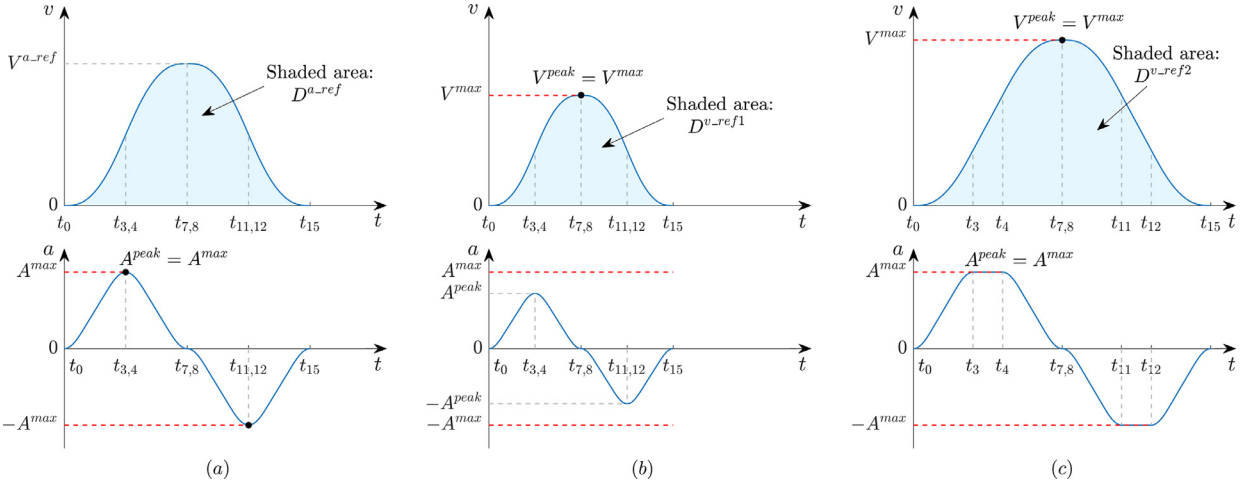

Fig. 5. Reference critical values for trajectory type evaluation.

travelled distance or low velocity limitation. Likewise, the constant velocity time period T_4 is unnecessary for the case of a short travelled distance. For more clarity, the computation starts with the definition of several reference critical values:

(1) Disregarding the velocity bound and target displacement, when the acceleration reaches its maximum allowable value $A^{\max}$, the velocity profile declines to zero with a symmetrical shape in the shortest time under the given acceleration and jerk limits, as indicated in Fig. 5(a). The corresponding peak velocity and the displacement covered are defined as V^{a_ref} and D^{a_ref}, respectively. More clearly, V^{a_ref} and D^{a_ref} are the minimum velocity and displacement that allow the acceleration to reach its limit value, so the motions with target displacements less than D^{a_ref} or velocity limits lower than V^{a_ref} should be accomplished with $|A^{peak}| < A^{\max}$.

(2) Disregarding the target displacement, when the velocity reaches its maximum allowable value $V^{\max}$, the velocity profile declines to zero with a symmetrical shape in the shortest time under the given acceleration and jerk limits, as indicated in Fig. 5(b) and (c). Two cases are further distinguished here based upon the relationship between the velocity bound $V^{\max}$ and the critical value V^{a_ref}. The corresponding displacements covered in the cases of $V^{\max} < V^{a\_ref}$ and $V^{\max} \geq V^{a\_ref}$ are respectively defined as D^{v_ref1} and D^{v_ref2}, which are essentially the minimum displacements that allow the velocity to reach its limit value. The motions with target displacements less than D^{v_ref1} or D^{v_ref2} should be accomplished with $|V^{peak}| < V^{\max}$.

These reference critical values are not totally independent of each other; the relation $D^{v\_ref2} \geq D^{a\_ref}$ is entailed by the condition $V^{\max} \geq V^{a\_ref}$, and the relation $D^{v\_ref1} < D^{a\_ref}$ is entailed by the condition $V^{\max} < V^{a\_ref}$. The expressions of the critical values will be provided below with the solutions of time parameters for different trajectory types to illustrate their derivation. Note that in practical algorithm implementation, these expressions are computed prior to the time parameters to evaluate the trajectory type. There are four types of motion profiles that can be summed up depending on the range of the given constraints.

Type I: $A^{\max}$attainable, $V^{\max}$ attainable ($|A^{peak}| = A^{\max}$, $|V^{peak}| = V^{\max}$)

If $V^{\max} \geq V^{a\_ref}$ and $D \geq D^{v\_ref2}$, the target displacement is large enough for planning the motion with the maximum allowable acceleration and velocity. In addition, the maximum allowable acceleration is achieved ahead of the maximum allowable velocity, so all four time periods exist in the profile (Fig. 6(a)). The equality condition in the judgement criteria

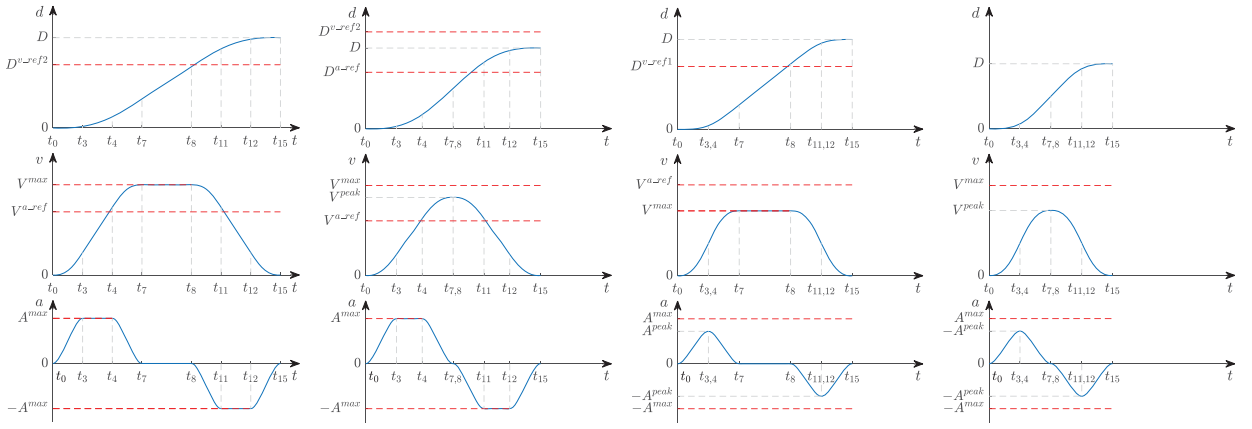

Fig. 6. Motion profiles for different trajectory types.

represents the critical case in which the corresponding limit is reached at only one point on the profile. For this trajectory type, the lengths of the sine and constant jerk time periods are determined by the acceleration limit $A^{\max}$, and the constant acceleration time period is determined by the velocity limit $V^{\max}$.

By substituting Eq. (19) into Eq. (8), T_1 and T_2 are found as follows:

$$T_1 = \frac{\pi\alpha A^{\max}}{(4\alpha+\pi-\pi\alpha)J^{\max}} \tag{20}$$

$$T_2 = \frac{\pi(1-\alpha)A^{\max}}{(4\alpha+\pi-\pi\alpha)J^{\max}} \tag{21}$$

Once T_1 and T_2 are obtained, referring to Eq. (13), T_3 is easily calculated as:

$$T_3 = \frac{V^{\max}}{A^{\max}} - (2T_1+T_2) = \frac{V^{\max}}{A^{\max}} - \frac{\pi(1+\alpha)A^{\max}}{(4\alpha+\pi-\pi\alpha)J^{\max}} \tag{22}$$

Then, from Eq. (15), the constant velocity time period satisfying the displacement requirement D is given by:

$$T_4 = \frac{D}{V^{\max}} - (4T_1+2T_2+T_3) = \frac{D}{V^{\max}} - \frac{V^{\max}}{A^{\max}} - \frac{\pi(1+\alpha)A^{\max}}{(4\alpha+\pi-\pi\alpha)J^{\max}} \tag{23}$$

Now, given that the time parameters are already defined, the critical values of interest V^{a_ref} and D^{v_ref2} can be formulated as follows:

$$V^{a\_ref} = A^{\max}(2T_1+T_2) = \frac{\pi(1+\alpha)(A^{\max})^2}{(4\alpha+\pi-\pi\alpha)J^{\max}} \tag{24}$$

$$D^{v\_ref2} = V^{\max}(4T_1+2T_2+T_3) = \frac{\pi(1+\alpha)A^{\max}V^{\max}}{(4\alpha+\pi-\pi\alpha)J^{\max}} + \frac{(V^{\max})^2}{A^{\max}} \tag{25}$$

Type II: $A^{\max}$ attainable, $V^{\max}$ unattainable ($|A^{peak}| = A^{\max}$, $|V^{peak}| < V^{\max}$)

If $V^{\max} \geq V^{a\_ref}$ and $D^{a\_ref} \leq D < D^{v\_ref2}$, the actual peak acceleration is not restricted by either the displacement requirement or the velocity bound. However, the trajectory achieves the target displacement before reaching the maximum allowable velocity, so there is no constant velocity phase, and $T_4 = 0$ Fig. 6(b)). The sine and constant jerk time periods are determined by the acceleration limit $A^{\max}$, and the constant acceleration time period is determined by the target displacement D. Hence, T_1 and T_2 can still be calculated by Eqs. (20) and ((21).

According to Eq. (15), the relation between the target displacement and the time period of constant acceleration may be expressed as:

$$D = A^{\max}\left({T_3}^2 + 6T_1T_3 + 3T_2T_3 + 8{T_1}^2 + 8T_1T_2 + 2{T_2}^2\right) \tag{26}$$

Solving this equation leads to the solution of T_3:

$$T_3 = -\left(3T_1 + \frac{3T_2}{2}\right) + \sqrt{\left(T_1+\frac{T_2}{2}\right)^2 + \frac{D}{A^{\max}}} = -\frac{3\pi(1+\alpha)A^{\max}}{2(4\alpha+\pi-\pi\alpha)J^{\max}} + \sqrt{\left[\frac{\pi(1+\alpha)A^{\max}}{2(4\alpha+\pi-\pi\alpha)J^{\max}}\right]^2 + \frac{D}{A^{\max}}} \tag{27}$$

Meanwhile, the involved critical value D^{a_ref} determined by $A^{\max}$ can be calculated by the following formula:

$$D^{a\_ref} = V^{a\_ref}(4T_1+2T_2) = \frac{2\pi^2(1+\alpha)^2(A^{\max})^3}{(4\alpha+\pi-\pi\alpha)^2(J^{\max})^2} \tag{28}$$

Type III: $A^{\max}$ unattainable, $V^{\max}$ attainable ($|A^{peak}| < A^{\max}$, $|V^{peak}| = V^{\max}$)

If $V^{\max} < V^{a\_ref}$ and $D \geq D^{v\_ref1}$, although the target displacement is large enough, the actual peak acceleration is restricted by the velocity limit $V^{\max}$ since the velocity limit is too small relative to the acceleration limit. The maximum allowable velocity is reached before the maximum allowable acceleration, giving rise to the disappearance of the constant acceleration phase, namely, $T_3 = 0$, while the constant velocity phase is further needed to achieve the target displacement Fig. 6(c)). To calculate the sine and constant jerk time periods determined by $V^{\max}$, combining Eqs. (13) and ((19) yields the following relation:

$$V^{\max} = J^{\max}\left[\frac{8}{\pi} + \frac{4(1-\alpha)}{\pi\alpha} + \frac{2(1-\alpha)}{\alpha} + \frac{(1-\alpha)^2}{\alpha^2}\right]{T_1}^2 \tag{29}$$

from which we have:

$$T_1 = \sqrt{\frac{\pi\alpha^2 V^{\max}}{(4\alpha + \pi - \pi\alpha)(\alpha+1)J^{\max}}} \tag{30}$$

$$T_2 = \sqrt{\frac{\pi(1-\alpha)^2 V^{\max}}{(4\alpha + \pi - \pi\alpha)(\alpha+1)J^{\max}}} \tag{31}$$

Consequently, using Eq. (15) where T_1 and T_2 are now known, the time period T_4 for the given target displacement D is solved by:

$$T_4 = \frac{D}{V^{\max}} - (4T_1 + 2T_2) = \frac{D}{V^{\max}} - \sqrt{\frac{4\pi(\alpha+1)V^{\max}}{(4\alpha + \pi - \pi\alpha)J^{\max}}} \tag{32}$$

Based on the above results, the corresponding critical values D^{v_ref1} determined by $V^{\max}$ can be derived as:

$$D^{v\_ref1} = V^{\max}(4T_1 + 2T_2) = \sqrt{\frac{4\pi(\alpha+1)(V^{\max})^3}{(4\alpha + \pi - \pi\alpha)J^{\max}}} \tag{33}$$

Type IV: $V^{\max}$ unattainable, $A^{\max}$ unattainable ($|A^{peak}| < A^{\max}$, $|V^{peak}| < V^{\max}$)

In case none of the above conditions is satisfied, that is, if $V^{\max} \geq V^{a\_ref}$ and $D < D^{a\_ref}$, or if $V^{\max} < V^{a\_ref}$ and $D < D^{v\_ref1}$, the profile belongs to type IV. Under the two conditions, the distance to travel is too short, and both the actual peak acceleration and velocity are constrained by the displacement requirement. Neither constant acceleration phases nor a constant velocity phase is needed in the trajectory, i.e., $T_3 = T_4 = 0$ (Fig. 6(d)). There are only the sine and constant jerk time periods, which are related to the target displacement D as:

$$D = J^{\max}\left[\frac{32{T_1}^3}{\pi} + \frac{8(1-\alpha)}{\alpha}{T_1}^3 + \frac{32(1-\alpha)}{\pi\alpha}{T_1}^3 + \frac{8(1-\alpha)^2}{\alpha^2}{T_1}^3 + \frac{8(1-\alpha)^2}{\pi\alpha^2}{T_1}^3 + \frac{2(1-\alpha)^3}{\alpha^3}{T_1}^3\right] \tag{34}$$

It follows that:

$$T_1 = \sqrt[3]{\frac{\pi\alpha^3 D}{2(4\alpha + \pi - \pi\alpha)(\alpha+1)^2 J^{\max}}} \tag{35}$$

$$T_2 = \sqrt[3]{\frac{\pi(1-\alpha)^3 D}{2(4\alpha + \pi - \pi\alpha)(\alpha+1)^2 J^{\max}}} \tag{36}$$

At this point, the minimum trajectory duration for an individual joint under different scenarios can be obtained. The values of the time parameters determined in this step are denoted by $T_{1,j}^{\min}$, $T_{2,j}^{\min}$, $T_{3,j}^{\min}$ and $T_{4,j}^{\min}$ to distinguish them from their final optimal values.

3.3. Adaptation for coordinated motion profiles

Typically, the minimized execution times $T_{joint,j}^{\min}$ for each joint trajectory individually achieved using the above algorithm are different, so the joints with shorter execution times will have reached the target positions while the others are still moving if all the joints execute the time optimal trajectories. Alternatively, smoother motion profiles can be planned by slowing them down to a new common duration to prevent unnecessary burden imposed on the actuators. The overall execution time for the synchronized motion is derived as:

$$T_{\mathrm{m}} = \max_j\left\{T_{joint,j}^{\min}\right\} \tag{37}$$

where $T_{joint,j}^{\min}$ ($j = 1, 2, \cdots, n$) represents the original calculated trajectory duration of joint j. T_m is the shortest time in which all the joints could accomplish the desired movements. Then, each time period of the minimum time trajectory for

Table 1
Geometric and inertial parameters and torque limits of the manipulator.

Joint No.	1	2	3	4	5	6
α_{i-1}(deg)	0	−90	−90	90	−90	90
a_{i-1}(m)	0	0	0	0	0	0
d_i(m)	0.177	0	0.450	0	0.412	0
θ_i(deg)	θ_1	θ_2+90	θ_3	θ_4	θ_5	θ_6
M (kg)	0.14	1.16	1.91	0.13	1.42	0.42
p_x(m)	0	0	−2.90e−3	0	0.04e−3	0.02e−3
p_y(m)	5.65e−3	19.52e−3	−0.81e−3	38.14e−3	0.91e−3	68.48e−3
p_z(m)	−39.01e−3	−0.26e−3	−116.39e−3	5.01e−3	−189.29e−3	−6.66e−3
I_{xx}(kg·m^2)	423.37e−6	3589.62e−6	25,698.56e−6	285.30e−6	26,462.23e−6	490.88e−6
I_{yy}(kg·m^2)	83.44e−6	1694.89e−6	25,309.98e−6	291.71e−6	26,265.26e−6	205.33e−6
I_{zz}(kg·m^2)	434.25e−6	2510.51e−6	1625.93e−6	76.68e−6	793.64e−6	410.95e−6
I_{xy}(kg·m^2)	0	0	4.51e−6	−0.01e−6	0	0
I_{yz}(kg·m^2)	−13.64e−6	−5.95e − 6	151.96e−6	10.97e−6	−249.37e−6	−14.36e−6
I_{xz}(kg·m^2)	0	0	386.78e−6	0.15e−6	0.05e−6	0
$\tau^{\max}$(N·m)	44.2	44.2	25.3	25.3	25.3	5.1

joint j is identically scaled up by a factor $K_j = T_m/T^{\min}_{joint,j}$ to accommodate this time while keeping the ramp coefficient unchanged.

In order for the displacement requirements to remain satisfied despite the above lengthening of their times, the extended joint trajectories should be performed with a reduced peak jerk in place of the jerk bound. Considering the relationship between the terminal displacement and the peak jerk reflected by Eq. (15), one obtains:

$$J_j^{peak} = \frac{d_{15,j}}{f_3\left(K_jT^{\min}_{1,j},\ K_jT^{\min}_{2,j},\ K_jT^{\min}_{3,j},\ K_jT^{\min}_{4,j}\right)} = \frac{d_{15,j}}{{K_j}^3 f_3\left(T^{\min}_{1,j},\ T^{\min}_{2,j},\ T^{\min}_{3,j},\ T^{\min}_{4,j}\right)} \tag{38}$$

From the above equation, it is known that the peak jerk J_j^{peak} of joint j varies correspondingly with a power of $1/K_j$ for the given target displacement, so this jerk is adjusted to $sign(q_{e,j}-q_{s,j})J_j^{\max}/{K_j}^3$.

As a result, the design steps of an optimal trajectory are outlined below: First, obtain the starting and ending positions in joint space, and set the kinematic bounds of each joint depending on actuator specifications and task type; moreover, choose an appropriate ramp coefficient α with a desired smoothness. Next, compute the critical reference values $V_j^{a\_ref}$ and $D_j^{a\_ref}$ as per Eqs. (24) and (28) for each joint. If $V_j^{\max} \geq V_j^{a\_ref}$, then $D_j^{v\_ref1}$ is calculated from Eq. (33); otherwise, D^{v_ref2} is calculated from Eq. (25). Given the criteria conditions, the trajectory type is evaluated according to the range of specified constraints, followed by determination of the primary time parameters. Subsequently, with the durations of the time optimal trajectories $T^{\min}_{joint,j}$ known for all joints, the common execution time T_m is derived referring to Eq. (37). The motion parameters of the involved joints are tuned to comply with this fixed time constraint, and finally, algebraic integration of the jerk profile defined in Eq. (3) yields the acceleration, velocity and displacement trajectories of the robot.

4. Case study

Experimental studies have been carried out on a self-developed robotic platform to evaluate the effectiveness and validity of the proposed approach. As depicted in Fig. 7(a), the robot is a serial revolute-joint anthropomorphic manipulator driven by smart digital Dynamixel Pro servo actuators from Robotis operating in position control mode. Fig. 7(b) gives the topology structure and link coordinate frames of the robot, and its geometric and inertial arm parameters are listed in Table 1. Each actuator contains a complete module integrating a direct current (DC) motor, reduction gear, controller, driver, sensor and network interface in one compact package, which provides a convenient tool for constructing robotic systems. All the actuators are interconnected with a daisy chain architecture via a half-duplex RS485 multidrop bus, allowing for independent control of each joint with a common wiring (see Fig. 7(c)). A personal computer is used to handle the data and control the actuators of the robot based on the Matlab development environment and the accompanying Dynamixel SDK provided by Robotis. Communication between the host computer and the actuators is established through a USB2Dynamixel serial adapter attached to the USB port of the computer.

For each task, the planning algorithm is implemented on the host computer to generate reference trajectories of the joints. Then the computer sends the position and velocity commands to the actuators via suitably addressed data packets to drive the device and reads their status. The transfer from the initial to the final posture should be performed in a smooth way without violating kinematic constraints imposed on the velocity, acceleration and jerk of each joint. Two groups of task data are adopted in this work as tabulated in Tables 2 and 3 to benchmark against other classic polynomial or trigonometric function-based trajectory planning methods that provide continuous jerk in earlier studies, namely, the seventh order polynomial [9] and 3-phase sine jerk trajectories [50,51].

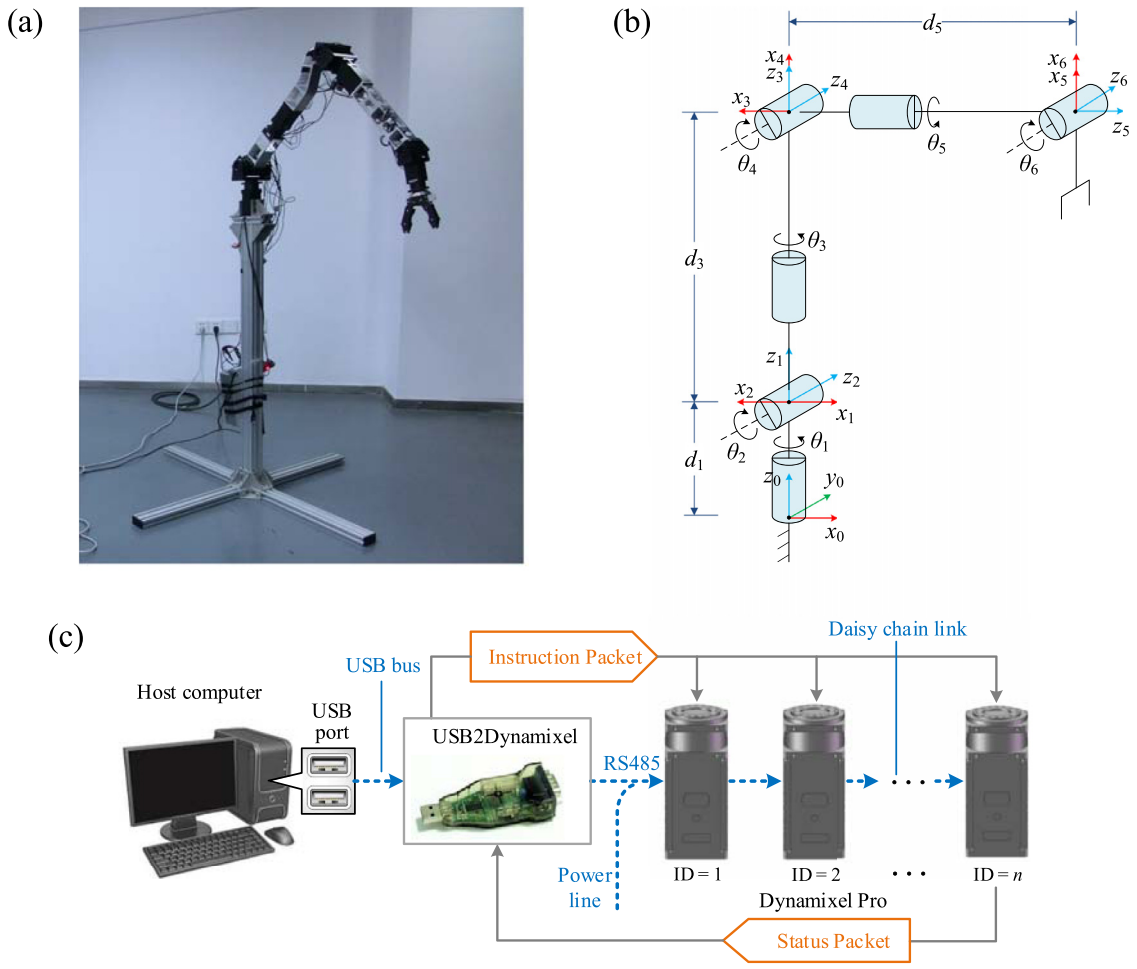

Fig. 7. Experimental platform: (a) robot manipulator; (b) topology structure and coordinate frames of the robot; (b) linking structure of the system.

Table 2
Desired positions and kinematic limits for task 1.

		Joint No.					
		1	2	3	4	5	6
Configuration (deg)	Start point	−10	20	15	150	30	120
	End point	55	35	30	10	70	25
Kinematic limits	Velocity (deg/s)	100	95	100	150	130	110
	Acceleration (deg/s^2)	60	60	75	70	90	80
	Jerk (deg/s^3)	60	66	85	70	75	70

As described in the previous section, the ramp coefficient α has the function of regulating the kinematic behavior of robots. Here, the values of $\alpha = 0.1$, 0.5 and 1 are applied to examine the impact of this parameter on the motion performance. The optimum execution times obtained by means of different techniques for the two tasks are summarized in Table 4. Note that for task 2, the algorithm of [50] fails to provide feasible trajectories that fulfill the displacement requirements as the constant velocity phase is required, showing its lack of universality.

The results show that the proposed approach is able to generate faster trajectories while all the joint limits are still complied with, ensuring that the robot runs within the safety range. In the event that α is set to 0.1 to assign a higher priority to efficiency, the resulting execution time decreases by 12% (from 4.6498 s to 4.0922 s) for task 1 and by 10.8% (from 2.1799s to 1.9441 s) for task 2 when taking the 3-phase sine jerk trajectory in [51], the best one among the considered benchmark methods as a reference. In particular, setting α to its limiting value zero leads to a bang-bang jerk profile with durations of 4 s and 1.9299 s, which are the shortest achievable times with limited jerk for the two tasks. Also notice that in task 1, the velocity and acceleration bounds are not attained due to the limitation of the prescribed displacements, so for the case of $\alpha = 1$, the same execution time as the result of [51] is achieved. In contrast, a time shortening of 6.2% is still obtained with $\alpha = 1$ in the second task, where the constant acceleration and velocity segments are present as the travelling distance is

Table 3
Desired positions and kinematic limits for task 2.

Joint		1	2	3	4	5	6
Configuration (rad)	Start point	$-\pi/3$	$\pi/6$	0	$-2\pi/5$	$\pi/4$	0
	End point	$2\pi/5$	$\pi/3$	$-\pi/6$	$-\pi/15$	$-\pi/2$	$\pi/4$
Kinematic limits	Velocity (rad/s)	1.8	2	1.5	2	2.5	2
	Acceleration (rad/s^2)	4	5	3.5	4	5	4
	Jerk (rad/s^3)	20	25	20	20	30	25

Table 4
Optimal execution time for the reference tasks.

Task	Work	Motion profile	Execution time (s)
1	Angeles [9]	4–5–6–7 Polynomial	4.7177
	Perumaal and Jawahar [50]	3-phase sine jerk (sync acc/dec)	7.5398
	Valente et al. [51]	3-phase sine jerk (async acc/dec)	4.6498
	Present	15-phase sine jerk	4.0922 ($\alpha = 0.1$)
			4.3875 ($\alpha = 0.5$)
			4.6498 ($\alpha = 1$)
2	Angeles [9]	4–5–6–7 Polynomial	2.7998
	Perumaal and Jawahar [50]	3-phase sine jerk (sync acc/dec)	N/A
	Valente et al. [51]	3-phase sine jerk (async acc/dec)	2.1799
	Present	15-phase sine jerk	1.9441 ($\alpha = 0.1$)
			1.9938 ($\alpha = 0.5$)
			2.0441 ($\alpha = 1$)

Table 5
Performance with degraded joints (task 2).

Degradation mode	Execution time (s)		Improvement
	Valente et al. [51]	Proposed ($\alpha = 0.5$)	
Nominal condition	2.1799	1.9938	8.5%
Degraded J5, jerk limit $30 \rightarrow 5$ rad/s^3	2.8719	2.7099	5.6%
Degraded J3, acc. limit $3.5 \rightarrow 0.6$ rad/s^2	2.6422	1.9938	24.5%
Degraded J1, vel. limit $1.8 \rightarrow 0.5$ rad/s	5.0040	4.9709	0.7%

long enough. This difference in efficiency would become more apparent when the magnitudes of the velocity or jerk limits are large relative to the acceleration limit values. Such a feature may be advantageous if the specific joints work in a degrading pattern under their nominal performance in the case that anomalies in the robot system such as undue component vibrations or motor temperature rise are detected as suggested in [51], for which an instance regarding task 2 is displayed in Table 5. The motion strategy presented shows an improvement in terms of reduced execution time, especially when the robot performs operations with an acceleration-degraded mode. This observation highlights the adaptation performance of the overall synchronization with optimality provided by the method, which minimizes undesirable influence brought by the degrading phenomena.

To illuminate more clearly the different abilities of these methods in exploiting the kinematic bounds, Fig. 8 provides a comparison of the velocity, acceleration and jerk trajectories of the joints that determine the execution time T_m (joint 4 in task 1 and joint 1 in task 2) produced by them. As shown in Fig. 8, the seventh-order polynomial model does not possess a constant velocity phase, so its maximum kinematic values exhibit a proportional relationship with respect to the trajectory duration given the target displacement. Theoretically speaking, only one of the kinematic bounds can be attained, which causes a remarkably slower movement in task 2 since the acceleration and jerk evolutions are severely constrained by the velocity bound. The traditional sine jerk model suffers from a similar issue, making it unable to achieve a full exploitation of its jerk range in task 2. Unlike these two models, the designed 15-phase sine jerk model allows the maximum jerk and acceleration to be maintained for the longest possible period such that the driving capabilities of joint actuators could be taken advantage of at a higher level to accelerate the movement.

Regarding the computation effort for these methods, Table 6 summarizes the average computing times obtained in 50 independent runs on the host computer with an Intel Core i7-6700k 4 GHz processor and 8 GB RAM. A considerably longer computing time is recorded for the method in [51] than for the other methods. This is readily understood since the method in [51] requires a numerical technique (active-set algorithm), while the others provide analytical solutions. Additionally, as the proposed method comprises more parameters to be solved, its computational speed is slightly slower than that of [9], but the difference is negligible compared to the reduced trajectory duration. The superiority of the analytical solution is that it ensures infinite resolution of the results and efficient computation, thus allowing prompt trajectory generation or replanning when the task requirements are changed or any anomalous status is detected. In contrast, a numerical method involves

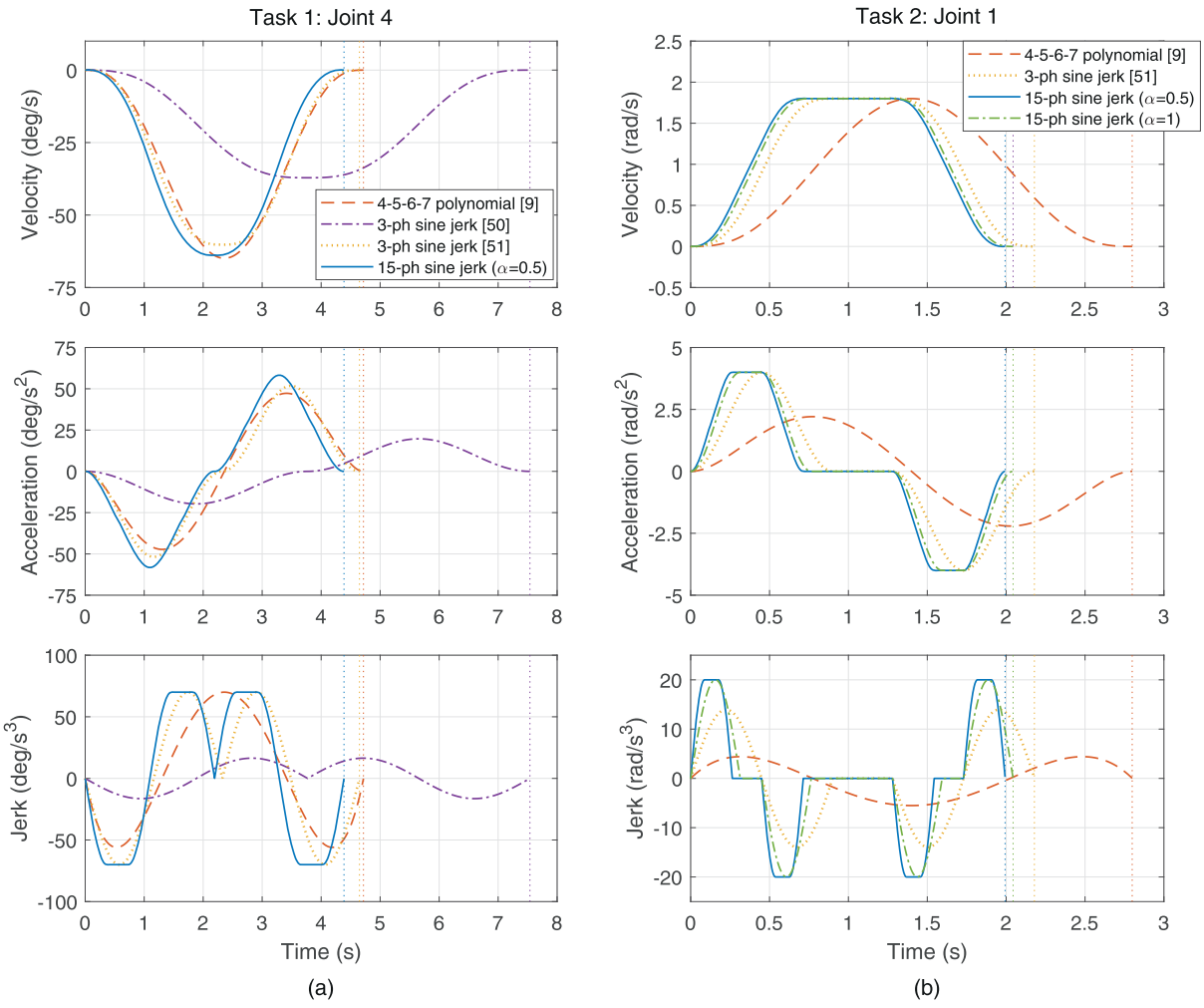

Fig. 8. Comparative trajectories of (a) joint 4 in task 1 and (b) joint 1 in task 2 obtained from different planning methods.

Table 6
Computational time for various methods.

Algorithm	Average Computing time (ms)		Solution type	Risk of failure
	Task 1	Task 2		
Angeles [9]	0.17	0.17	Analytical	No
Perumaal and Jawahar [50]	0.25	N/A	Analytical	Yes
Valente et al. [51]	46	61	Numerical	Yes
Present ($\alpha = 0.5$)	0.28	0.31	Analytical	No

an unpredictable iterative procedure and computation time and may have the potential to fail due to the unsuitable choice of the initial solution. All the techniques appear acceptable for online use purely in terms of absolute computation time (within 100 ms) without considering the reliability, but notice that the algorithms were implemented on a computer that has powerful data-handling ability. In fact, the average computational time required by the algorithm of [51] is two orders of magnitude longer than that of the proposed approach. When the algorithms are implemented by low-cost processors commonly used in industry, the gap in absolute time is notably enlarged.

Apart from improved efficiency, another advantage of the 15-phase sine jerk trajectory lies in the suppression of the jerk values. Table 7 reports the maximum jerks of each joint and their average values for the 3-phase [51] and 15-phase sine jerk trajectories ($\alpha = 1$). As portrayed in Table 7, except for the joints that determine the execution time, the 15-phase sine jerk profile achieves a reduction in most of the maximum joint jerk values relative to the 3-phase sine jerk profile, even when the former leads to a shorter execution time in task 2. Specifically, the overall average values of the resulting

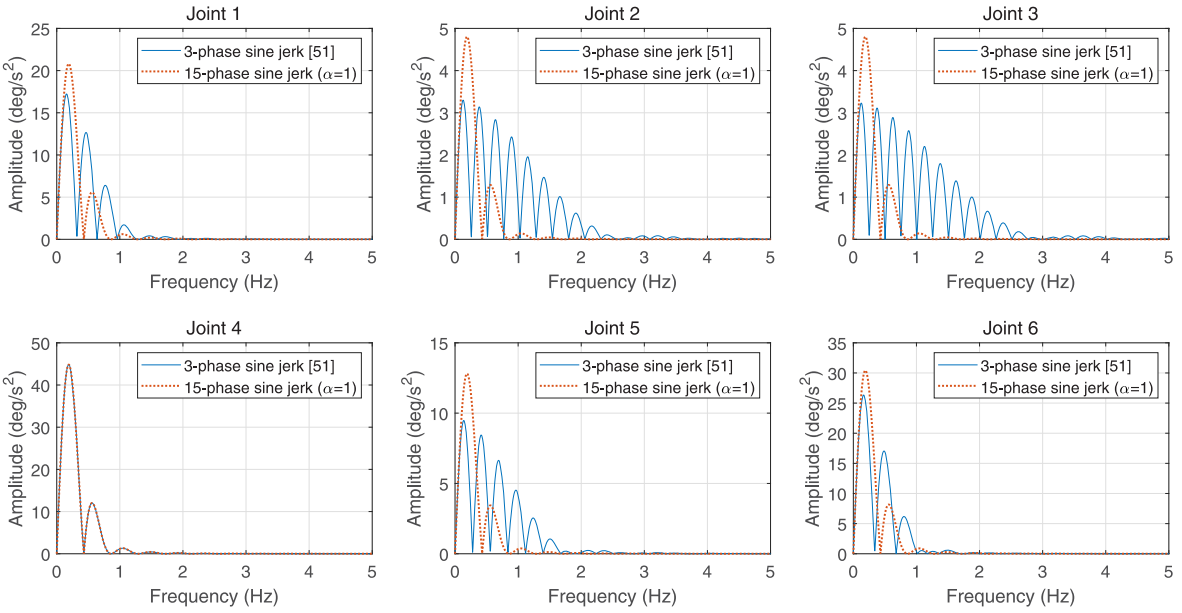

Fig. 9. Acceleration's frequency spectrum comparison for the two sine jerk techniques for task 1.

Table 7
Maximum jerk values for the two sine jerk techniques.

Task	Algorithm	j^{max} (Task 1: deg/s^3, Task 2: rad/s^3)						
		Joint 1	Joint 2	Joint 3	Joint 4	Joint 5	Joint 6	Average
1	Valente et al. [51]	56.31	41.63	52.31	70.00	61.27	69.79	58.55
	Proposed ($\alpha = 1$)	32.50	7.50	7.50	70.00	20.00	47.50	30.83
2	Valente et al. [51]	13.96	21.57	17.68	19.76	21.86	21.89	19.45
	Proposed ($\alpha = 1$)	20.00	3.08	3.08	6.22	17.39	4.72	9.08

Table 8
Mean jerk values for the two sine jerk techniques.

Task	Algorithm	j^{mean} (Task 1: deg/s^3, Task 2: rad/s^3)						
		Joint 1	Joint 2	Joint 3	Joint 4	Joint 5	Joint 6	Average
1	Valente et al. [51]	23.48	8.70	9.64	44.56	17.96	32.56	22.82
	Proposed ($\alpha = 1$)	20.69	4.77	4.77	44.56	12.73	30.23	19.63
2	Valente et al. [51]	7.34	3.57	3.26	5.04	8.55	4.49	5.38
	Proposed ($\alpha = 1$)	7.82	1.96	1.96	3.59	6.80	2.57	4.12

maximum jerks are 47.3% and 53.3% lower than those of [51] for the two tasks. Table 8 reports the mean joint jerks and their average values along the whole trajectory compared with those obtained by [51]. Similarly, the technique described herein yields lower mean jerk values for almost all of the joints, with the average percentage decrease being 14% and 23.4% in the two tasks. As the jerk amplitude has a tight correlation with the vibratory intensity of the structure, this benefit is of great significance for precise robot operations. The average values of the maximum and mean values of the velocity and acceleration are shown in Table 9. Since the robot executes point-to-point motions in the tasks, the mean velocities are inversely proportional to the execution time, so the two techniques produce the same mean joint velocities in task 1, and a slightly higher mean velocity is reported for the 15-phase trajectory in task 2. Moreover, with the 15-phase trajectory, the joint can be accelerated to a peak velocity more closely to its maximum permissible value thanks to a better exploitation of the jerk range. Additionally, the average maximum acceleration values are 14% and 28% lower than those of the 3-phase trajectory in the two tasks, while the average mean acceleration values are 20.5% and 43.4% higher.

Fig. 9 presents the corresponding frequency spectrum of the acceleration profiles with the two sine jerk techniques in task 1, which reflects the ideal stress exerted on the mechanical structure by the driving system during the motion. In such spectrograms, it is desirable that harmonic contents at high frequencies have smaller magnitudes. In fact, a lower

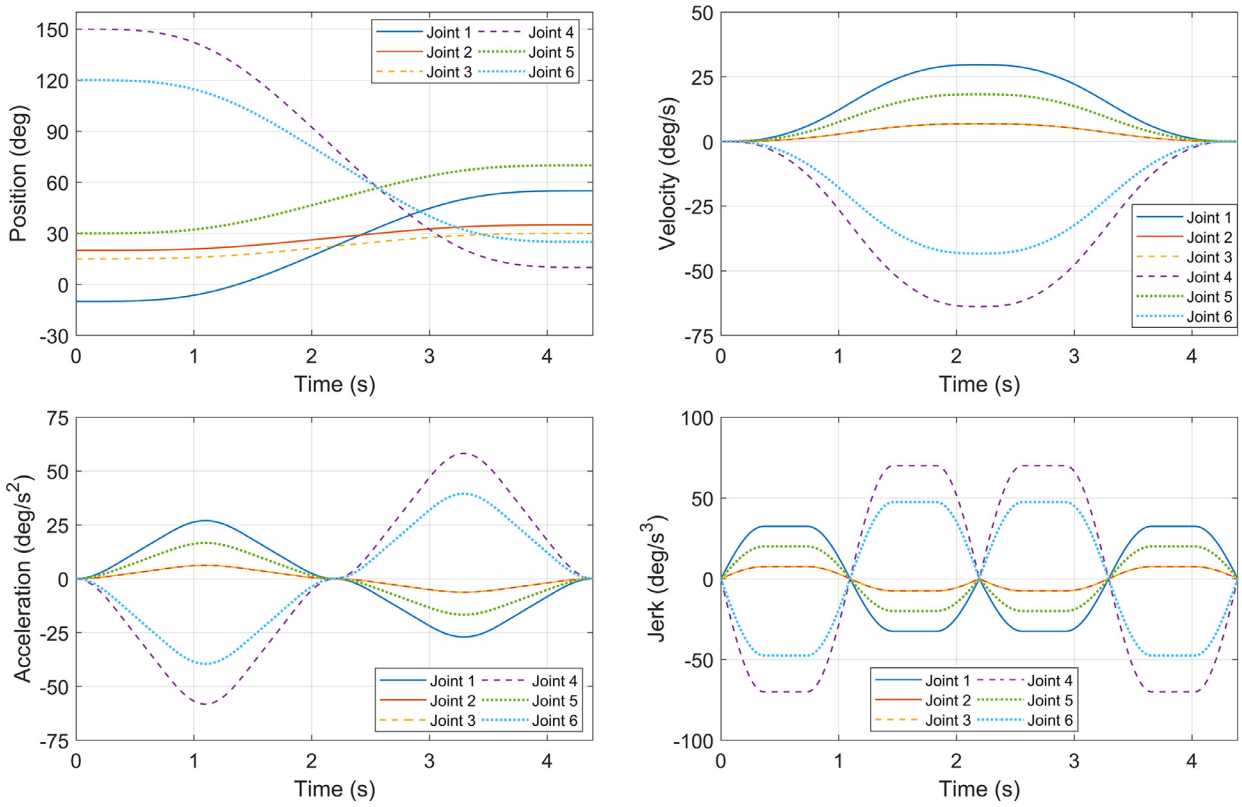

Fig. 10. Joint position, velocity, acceleration and jerk profiles (α=0.5) for task 1.

Table 9
Average maximum and mean velocity and acceleration values for the two sine jerk techniques.

Task	Algorithm	v^{max} (Task 1: deg/s, 2: rad/s)	v^{mean} (Task 1: deg/s, 2: rad/s)	a^{max} (Task 1: deg/s^2, 2: rad/s^2)	a^{mean} (Task 1: deg/s^2, 2: rad/s^2)
1	Valente et al. [51]	22.01	13.26	26.53	9.47
	Proposed ($\alpha = 1$)	26.52	13.26	22.82	11.41
2	Valente et al. [51]	0.82	0.58	2.93	0.76
	Proposed ($\alpha = 1$)	1.12	0.61	2.11	1.09

high-frequency harmonic content signifies a smoother motion profile in the time domain. Dramatic variations or discontinuities in the acceleration profile make the spectrum present relevant terms at high frequencies. In this event, a wider bandwidth of the amplitude spectrum could stimulate the resonance frequencies of the mechanical structure and accordingly induce vibrations. Note that for most joints, although the main lobes of the 15-phase sine jerk trajectory have a peak value larger than those of the 3-phase sine jerk trajectory, the side lobes are appreciably smaller and vanish at lower frequencies. Therefore, the 15-phase sine jerk trajectory is more suitable for applications where high frequencies must not be excited.

Figs. 10 and 11 illustrate in detail the profiles of joint position, velocity, acceleration and jerk planned using the proposed technique with $\alpha = 0.5$ for the two tasks. The plots reveal that all the motion curves remain continuous and bounded within the specified allowable ranges at all times, guaranteeing adequate smoothness of the optimized trajectory. The joints reach the desired positions monotonically without any oscillation. Then, the planning data are transmitted to the controllers inside the actuators to drive the robotic manipulator to maneuver along the desired trajectory. The reference versus the measured positions by the built-in encoders of joints 1 and 3 for task 2, together with the corresponding tracking errors, are given in Fig. 12, from which it can be seen that the actual measured curves are fairly close to the reference ones, with generally good consistency except for a slight time delay because of the PID control scheme. The largest tracking errors during the movement for the two joints are approximately 2.87° and −0.91°, and the final positioning errors at the

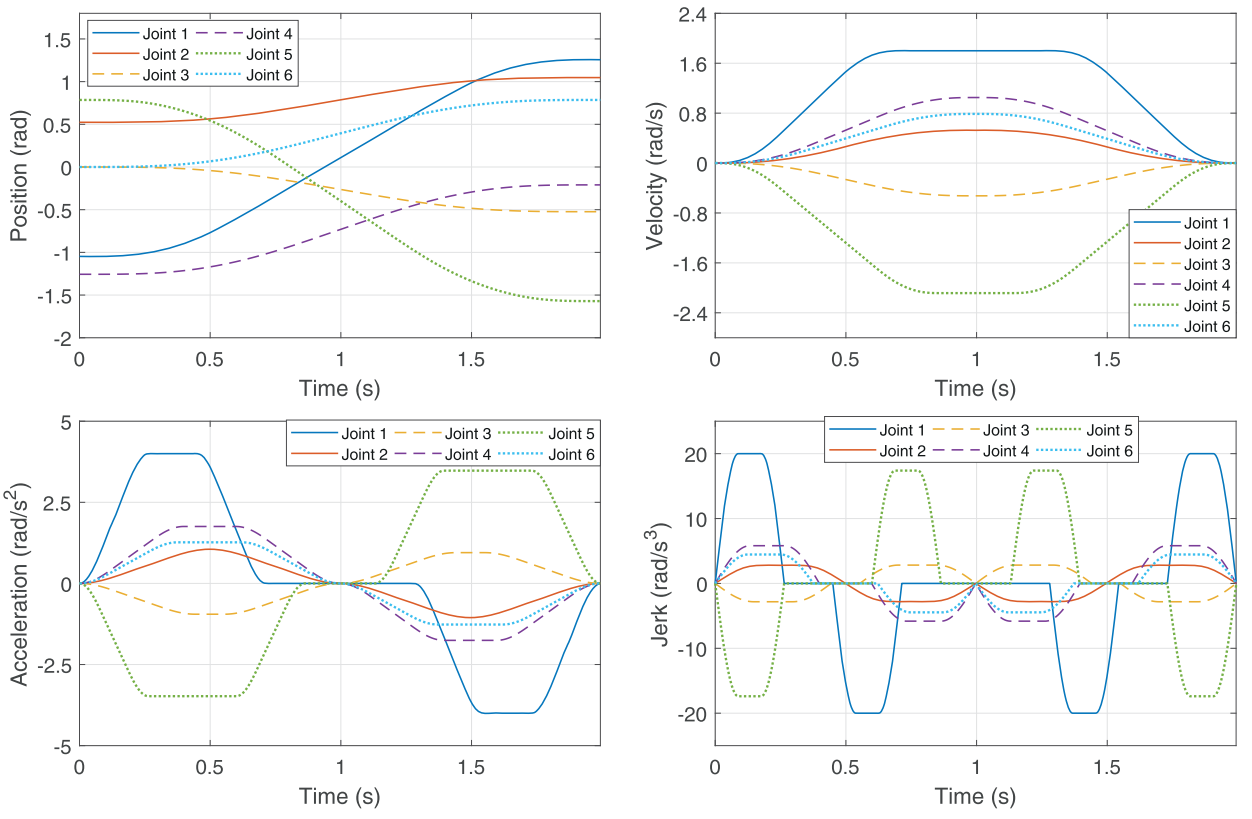

Fig. 11. Joint position, velocity, acceleration and jerk profiles (α=0.5) for task 2.

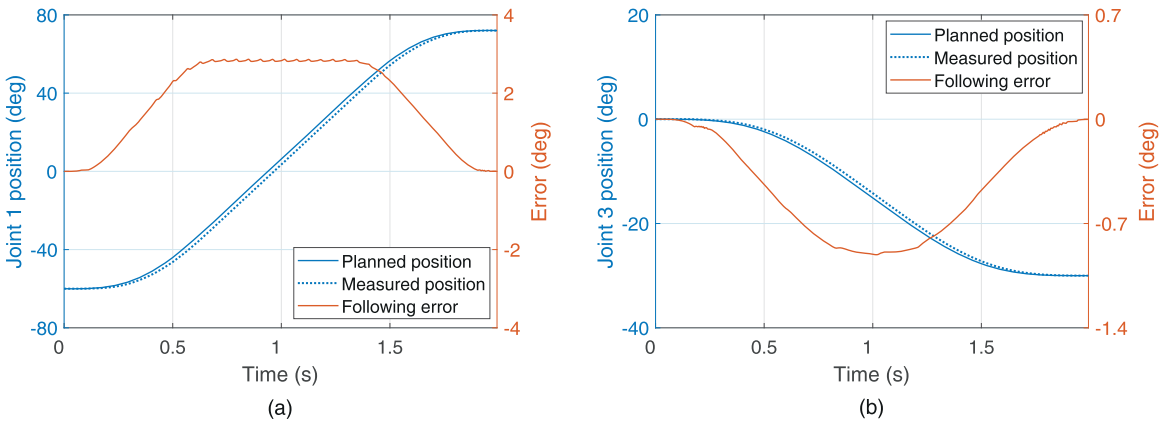

Fig. 12. Measured joint position profiles of (a) joint 1 and (b) joint 3 for task 2.

destination points converge to nearly zero. The torque profiles of the joint actuators are reported in Fig. 13. The torque profiles change smoothly without any saturation throughout the motion as a result of continuous acceleration and jerk. Even though all the kinematic bounds are reached, there is still a certain gap between the peak torques and the torque limits. Due to the continuous torque required by the trajectory, the trajectory can be followed by the manipulator precisely with ease. The tracking performance may be further enhanced by the adoption of an advanced control strategy. Satisfactory results have been achieved in experiments on a manipulator system, thus validating the practicability of the proposed methodology.

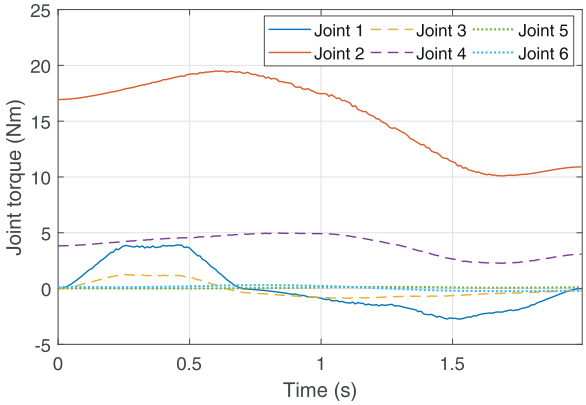

Fig. 13. Joint actuator torque profiles for task 2.

5. Conclusions

The design and computation of optimal reference motion profiles for industrial robots is a challenging task, which necessitates a reasonable balance among the speed, precision and complexity. Against this background, jerk-bounded trajectories as a suitable choice have drawn increasing attention in recent years. Previous works providing continuous jerk usually suffer from insufficient exploitation of kinematic limits or incomplete solutions for potential trajectory types. The main contribution of this work is the development of a smooth trajectory planning method for robot manipulators to minimize trajectory durations by adopting a modified sine jerk model that aims to make maximum use of the joint performance while maintaining good smoothness. Experiments conducted on a manipulator confirm the effectiveness and utility of the proposed approach. The features of the proposed methodology can be summarized as follows:

(1) The execution times of the produced trajectories are effectively reduced without compromising the level of continuity compared to that of jerk-continuous algorithms from previous studies. This approach yields execution times up to 12% and 24.5% shorter, respectively, for normal and degraded modes than the best benchmark method [51]. This seems to be conductive to enhanced productivity in precise applications from an industrial point of view.
(2) The generated velocity, acceleration and jerk profiles of each joint are all continuous and strictly bounded within the imposed constraints, which is beneficial to the positioning and tracking accuracy.
(3) As an average decrease of up to 23.4% of jerk amplitudes can be expected in comparison with those of [51], the harmonic contents of the acceleration profiles have smaller magnitudes at higher frequencies, thus preventing the excitation of mechanical resonance modes of the structure.
(4) The ramp coefficient introduced offers the possibility to fine-tune the kinematic behavior according to actual needs, trading off speed and motion smoothness, which represents a key competitive opportunity for robots.
(5) This method proposes a complete analytical solution by evaluating the trajectory type through a priori defined constraint criteria, ensuring an efficient and reliable determination of the motion trajectory parameters without potential risk of failure. The computing time is two orders of magnitude lower than that of [51]. Hence, the method is well suited for applications that require online trajectory computation and updating in manufacturing plants.

The major directions of potential future research address the following issues. This work focuses on the trajectory planning method for online use, so the optimization considers only the kinematic constraints to ensure computational efficiency. As the acceleration limits are actually position dependent based on the maximum actuator forces/torques, incorporating a dynamical model would allow better utilization of the manipulator capability compared to purely kinematic trajectory planning. Future work will focus on an offline algorithm that formulates dynamic constraints to further improve the performance for trajectory planning with multiple optimization objectives, such as torque or energy minimization. Furthermore, the designed trajectory model can be generalized to the case with arbitrary states at the endpoints for motion planning of more complicated time-varying parametric paths in operational space. The experimental validation will also be performed on more types of robots such as parallel robots and flexible robots.

Declaration of Competing Interest

None.

Acknowledgements

This work was supported by Special Program for Innovation Method of the Ministry of Science and Technology, China (2018IM020100), National Natural Science Foundation of China (51975360, 51775332, 51975350, 51675329), National Social Science Foundation of China (17ZDA020).

References

[1] M. Moghaddam, S.Y. Nof, Parallelism of pick-and-place operations by multi-gripper robotic arms, Robot. Comput. Integr. Manuf. 42 (2016) 135–146 https://doi.org/10.1016/j.rcim.2016.06.004.
[2] M.H. Korayem, S.F. Dehkordi, Dynamic modeling of flexible cooperative mobile manipulator with revolute-prismatic joints for the purpose of moving common object with closed kinematic chain using the recursive Gibbs–Appell formulation, Mech. Mach. Theory. 137 (2019) 254–279 https://doi.org/10.1016/j.mechmachtheory.2019.03.026.
[3] J. Wu, G. Yu, Y. Gao, L. Wang, Mechatronics modeling and vibration analysis of a 2-DOF parallel manipulator in a 5-DOF hybrid machine tool, Mech. Mach. Theory 121 (2018) 1339–1351 https://doi.org/10.1016/j.mechmachtheory.2017.10.023.
[4] H.J. Heo, Y. Son, J.M. Kim, A trapezoidal velocity profile generator for position control using a feedback strategy, Energies 12 (2019) 1222 https://doi.org/10.3390/en12071222.
[5] D.K. Thomsen, R.S. Knudsen, D. Brandt, O. Balling, X. Zhang, Generating vibration free rest-to-rest trajectories for configuration dependent dynamic systems via 3-segmented input shaping, in: Proc. - IEEE Int. Conf. Robot. Autom., IEEE, 2018, pp. 4361–4366. https://doi.org/10.1109/ICRA.2018.8460865.
[6] J. Wu, D. Wang, L. Wang, A control strategy of a two degrees-of-freedom heavy duty parallel manipulator, J. Dyn. Syst. Meas. Control. Trans. ASME. 137 (2015) 61007 https://doi.org/10.1115/1.4029244.
[7] M.H. Korayem, H.N. Rahimi, A. Nikoobin, Mathematical modeling and trajectory planning of mobile manipulators with flexible links and joints, Appl. Math. Model. 36 (2012) 3229–3244 https://doi.org/10.1016/j.apm.2011.10.002.
[8] A. Gasparetto, V. Zanotto, Optimal trajectory planning for industrial robots, Adv. Eng. Softw. 41 (2010) 548–556 https://doi.org/10.1016/j.advengsoft.2009.11.001.
[9] J. Angeles, Fundamentals of robotic mechanical systems, springer international publishing, Cham (2014) https://doi.org/10.1007/978-3-319-01851-5.
[10] A. Gasparetto, P. Boscariol, A. Lanzutti, R. Vidoni, Path planning and trajectory planning algorithms: a general overview, Mech. Mach. Sci. (2015) 3–27 https://doi.org/10.1007/978-3-319-14705-5_1.
[11] D. Constantinescu, Smooth time optimal trajectory planning for industrial manipulators, (1998). https://doi.org/10.14288/1.0088569.
[12] K.J. Kyriakopoulos, G.N. Saridis, Minimum jerk path generation., in: IEEE, 1988: pp. 364–369. https://doi.org/10.1109/robot.1988.12075.
[13] V. Zanotto, A. Gasparetto, A. Lanzutti, P. Boscariol, R. Vidoni, Experimental validation of minimum time-jerk algorithms for industrial robots, J. Intell. Robot. Syst. Theory Appl. 64 (2011) 197–219 https://doi.org/10.1007/s10846-010-9533-5.
[14] P. Besset, R. Béarée, FIR filter-based online jerk-constrained trajectory generation, Control Eng. Pract 66 (2017) 169–180.
[15] J. Huang, P. Hu, K. Wu, M. Zeng, Optimal time-jerk trajectory planning for industrial robots, Mech. Mach. Theory 121 (2018) 530–544 https://doi.org/10.1016/j.mechmachtheory.2017.11.006.
[16] M. Arsenault, L.F. Tremblay, M. Zeinali, Optimization of trajectory durations based on flow rate scaling for a 4-DoF semi-automated hydraulic rock-reaker, Mech. Mach. Theory 143 (2020) 103632 https://doi.org/10.1016/j.mechmachtheory.2019.103632.
[17] D. Richiedei, A. Trevisani, Analytical computation of the energy-efficient optimal planning in rest-to-rest motion of constant inertia systems, Mechatronics 39 (2016) 147–159 https://doi.org/10.1016/j.mechatronics.2016.05.004.
[18] T. Huang, P.F. Wang, J.P. Mei, X.M. Zhao, D.G. Chetwynd, Time minimum trajectory planning of a 2-DOF translational parallel robot for pick-and-place operations, CIRP Ann. - Manuf. Technol. 56 (2007) 365–368 https://doi.org/10.1016/j.cirp.2007.05.085.
[19] W.P. Bailón, E.B. Cardiel, I.J. Campos, A.R. Paz, Mechanical energy optimization in trajectory planning for six DOF robot manipulators based on eighth-degree polynomial functions and a genetic algorithm, in: Progr. Abstr. B. - 2010 7th Int. Conf. Electr. Eng. Comput. Sci. Autom. Control. CCE 2010, IEEE, 2010, pp. 446–451. https://doi.org/10.1109/ICEEE.2010.5608583.
[20] H. Esfandiar, M. Habibnejad Korayem, M. Haghpanahi, Optimal trajectory planning for flexible mobile manipulators under large deformation using meta-heuristic optimization methods, ADMT J (2016) 9.
[21] A. Gallant, C. Gosselin, Extending the capabilities of robotic manipulators using trajectory optimization, Mech. Mach. Theory 121 (2018) 502–514 https://doi.org/10.1016/j.mechmachtheory.2017.09.016.
[22] H. Seki, S. Tadakuma, Conf. Proc. - IEEE Int. Conf. Syst. Man Cybern., IEEE (2004) 722–727 https://doi.org/10.1109/icsmc.2004.1398387.
[23] T. Su, L. Cheng, Y. Wang, X. Liang, J. Zheng, H. Zhang, Time-optimal trajectory planning for delta robot based on quintic pythagorean-hodograph curves, IEEE Access 6 (2018) 28530–28539 https://doi.org/10.1109/ACCESS.2018.2831663.
[24] S. Bureerat, N. Pholdee, T. Radpukdee, P. Jaroenapibal, Self-adaptive MRPBIL-DE for 6D robot multiobjective trajectory planning, Expert Syst. Appl 136 (2019) 133–144 https://doi.org/10.1016/j.eswa.2019.06.033.
[25] R. Saravanan, S. Ramabalan, C. Balamurugan, A. Subash, Evolutionary trajectory planning for an industrial robot, Int. J. Autom. Comput 7 (2010) 190–198 https://doi.org/10.1007/s11633-010-0190-8.
[26] B.I. Kazem, A.I. Mahdi, A.T. Oudah, Motion planning for a robot arm by using genetic algorithm, Jordan, J. Mech. Ind. Eng. (2008) 2 http://jjmie.hu.edu.jo/files/JJMIE-V2-N3-press/2(16-21).pdf.
[27] A. Visioli, Trajectory planning of robot manipulators by using algebraic and trigonometric splines, Robotica 18 (2000) 611–631 https://doi.org/10.1017/S0263574700002721.
[28] M.-.S. Huang, Y.-.L. Hsu, R.-.F. Fung, Minimum-energy point-to-point trajectory planning for a motor-toggle servomechanism, IEEE/ASME Trans. Mechatron. 17 (2011) 337–344.
[29] S. Fang, X. Ma, Y. Zhao, Q. Zhang, Y. Li, Trajectory planning for seven-DOF robotic arm based on quintic polynormial, in: Proc. - 2019 11th Int. Conf. Intell. Human-Machine Syst. Cybern. IHMSC 2019, Springer, 2019, pp. 198–201. https://doi.org/10.1109/IHMSC.2019.10142.
[30] Z. Xie, P. Wu, P. Ren, A comparative study on the pick-and-place trajectories for a delta robot, in: Proc. ASME Des. Eng. Tech. Conf., American Society of Mechanical Engineers Digital Collection, 2016.
[31] B.H. Chang, Y. Hori, Trajectory design considering derivative of jerk for head-positioning of disk drive system with mechanical vibration, IEEE/ASME Trans. Mechatron. 11 (2006) 273–279 https://doi.org/10.1109/TMECH.2006.875559.
[32] S. Kucuk, Maximal dexterous trajectory generation and cubic spline optimization for fully planar parallel manipulators, Comput. Electr. Eng. 56 (2016) 634–647 https://doi.org/10.1016/j.compeleceng.2016.07.012.
[33] S. Kucuk, Optimal trajectory generation algorithm for serial and parallel manipulators, Robot. Comput. Integr. Manuf. 48 (2017) 219–232 https://doi.org/10.1016/j.rcim.2017.04.006.
[34] A. Gasparetto, V. Zanotto, A new method for smooth trajectory planning of robot manipulators, Mech. Mach. Theory 42 (2007) 455–471 https://doi.org/10.1016/j.mechmachtheory.2006.04.002.
[35] B. Sencer, K. Ishizaki, Smooth polynomial interpolation for point-to-point trajectories with vibration avoidance, in: IECON 2015 - 41st Annu, in: Conf. IEEE Ind. Electron. Soc, IEEE, 2015, pp. 2070–2075. https://doi.org/10.1109/IECON.2015.7392406.
[36] M.T. Nguyen, J.H. Huang, Smooth and time optimal trajectory planning for industrial robot using a single polynomial, in: Lect. Notes Networks Syst., Springer, 2020, pp. 657–663. https://doi.org/10.1007/978-3-030-37497-6_76.

[37] R.F. Fung, Y.H. Cheng, Trajectory planning based on minimum absolute input energy for an LCD glass-handling robot, Appl. Math. Model. 38 (2014) 2837–2847 https://doi.org/10.1016/j.apm.2013.11.017.
[38] B. Siciliano, L. Sciavicco, L. Villani, G. Oriolo, Robotics: modelling, planning and control, Springer Sci. Bus. Media (2010).
[39] M. Boryga, A. Graboś, Planning of manipulator motion trajectory with higher-degree polynomials use, Mech. Mach. Theory 44 (2009) 1400–1419 https://doi.org/10.1016/j.mechmachtheory.2008.11.003.
[40] V. V H. Barghi, R Nabiyev, Benveniste, trajectory planning using high-order polynomials under acceleration constraint, J. Optim. Ind. Eng. 10 (2016) 1–6.
[41] R.A. Osornio-Rios, R. de Jesús Romero-Troncoso, G. Herrera-Ruiz, R. Castañeda-Miranda, FPGA implementation of higher degree polynomial acceleration profiles for peak jerk reduction in servomotors, Robot. Comput. Integr. Manuf. 25 (2009) 379–392 https://doi.org/10.1016/j.rcim.2008.01.002.
[42] H. Wang, H. Wang, J. Huang, B. Zhao, L. Quan, Smooth point-to-point trajectory planning for industrial robots with kinematical constraints based on high-order polynomial curve, Mech. Mach. Theory 139 (2019) 284–293 https://doi.org/10.1016/j.mechmachtheory.2019.05.002.
[43] J.-Y. Dieulot, I. Thimoumi, F. Colas, R. Béarée, Numerical aspects and performances of trajectory planning methods of flexible axes, Int. J. Comput. Commun. Control 1 (2006) 35 https://doi.org/10.15837/ijccc.2006.4.2304.
[44] H. Ouyang, N. Uchiyama, S. Sano, Residual vibration suppression conditions for mechanical system motion using simple trajectory, in: 2011 IEEE/SICE Int. Symp. Syst. Integr. SII 2011, 8, 2011, pp. 1067–1071. https://doi.org/10.1109/SII.2011.6147597.
[45] A. Abe, K. Hashimoto, A novel feedforward control technique for a flexible dual manipulator, Robot. Comput. Integr. Manuf. 35 (2015) 169–177 https://doi.org/10.1016/j.rcim.2015.03.008.
[46] D. Simon, C. Isik, Optimal trigonometric robot joint trajectories, Robotica 9 (1991) 379–386 https://doi.org/10.1017/S0263574700000552.
[47] A.C. Lee, M.T. Lin, Y.R. Pan, W.Y. Lin, The feedrate scheduling of NURBS interpolator for CNC machine tools, CAD Comput. Aided Des 43 (2011) 612–628 https://doi.org/10.1016/j.cad.2011.02.014.
[48] L. Biagiotti, C. Melchiorri, L. Moriello, Damped harmonic smoother for trajectory planning and vibration suppression, IEEE Trans. Control Syst. Technol. 28 (2020) 626–634 https://doi.org/10.1109/TCST.2018.2882340.
[49] Y. Wang, D. Yang, R. Gai, S. Wang, S. Sun, Design of trigonometric velocity scheduling algorithm based on pre-interpolation and look-ahead interpolation, Int. J. Mach. Tools Manuf 96 (2015) 94–105 https://doi.org/10.1016/j.ijmachtools.2015.06.009.
[50] S. Perumaal, N. Jawahar, Synchronized trigonometric S-curve trajectory for jerk-bounded time-optimal pick and place operation, Int. J. Robot. Autom. 27 (2012) 385–395 https://doi.org/10.2316/Journal.206.2012.4.206-3780.
[51] A. Valente, S. Baraldo, E. Carpanzano, Smooth trajectory generation for industrial robots performing high precision assembly processes, CIRP Ann. - Manuf. Technol. 66 (2017) 17–20 https://doi.org/10.1016/j.cirp.2017.04.105.
[52] H.Z. Li, Z.M. Gong, W. Lin, T. Lippa, Motion profile planning for reduced jerk and vibration residuals, SIMTech Tech. Rep. 8 (2007) 32–37 papers2://publication/uuid/FD6384DF-7479-45BC-A161-BB7169BBD6AF.
[53] L. Hongda, C. Hao, X. Xuecheng, Z. Wansheng, A jump motion velocity planning algorithm with continuous jerk for electrical discharge machining, Procedia CIRP 42 (2016) 547–551 https://doi.org/10.1016/j.procir.2016.02.249.